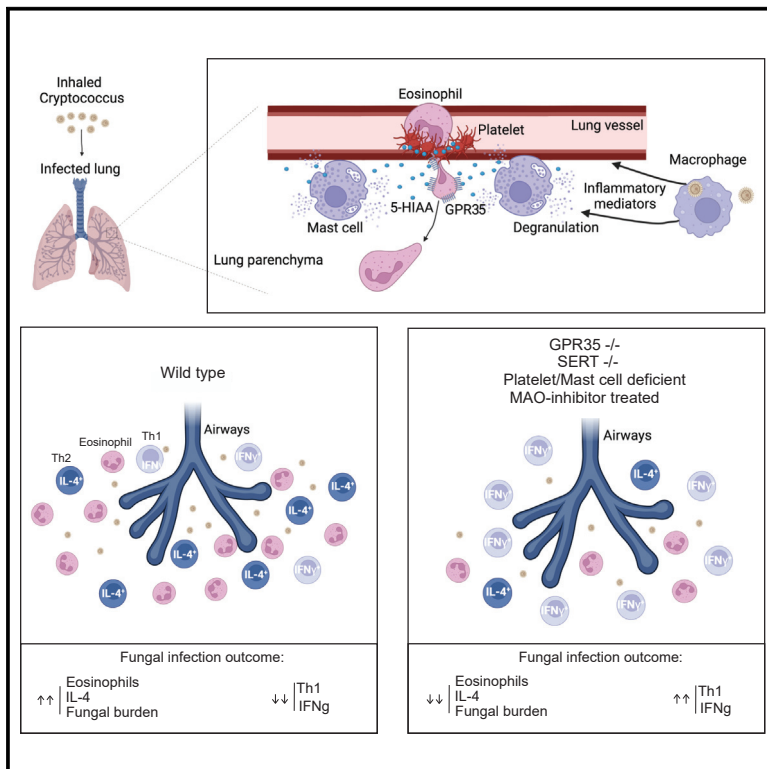


Platelets and mast cells promote pathogenic eosinophil recruitment during invasive fungal infection via the 5-HIAA-GPR35 ligand-receptor system

Graphical abstract



Authors

Marco De Giovanni, Eric V. Dang,
Kevin Y. Chen, Jinping An,
Hiten D. Madhani, Jason G. Cyster

Correspondence

marco.degiovanni@ucsf.edu (M.D.G.),
jason.cyster@ucsf.edu (J.G.C.)

In brief

Cryptococcus neoformans infection, a leading cause of fungal meningitis, involves pathogenic eosinophil accumulation. De Giovanni et al. reveal that the chemoattractant receptor GPR35 and its platelet- and mast-cell-derived ligand 5-hydroxyindoleacetic acid (5-HIAA), a serotonin metabolite, promotes eosinophil recruitment to the infected lung and exacerbation of disease. Modifiers of serotonin metabolism may be useful in the treatment of fungal infections.

Highlights

- GPR35 functions as a chemoattractant receptor in eosinophils
- 5-HIAA from platelets and mast cells helps recruit eosinophils to the inflamed lung
- GPR35⁺ eosinophil recruitment alters Th cell activity and reduces fungal clearance
- MAOIs reduce eosinophil recruitment and protect from *Cryptococcus* infection

Article

Platelets and mast cells promote pathogenic eosinophil recruitment during invasive fungal infection via the 5-HIAA-GPR35 ligand-receptor system

Marco De Giovanni,^{1,*} Eric V. Dang,² Kevin Y. Chen,¹ Jinping An,¹ Hiten D. Madhani,² and Jason G. Cyster^{1,3,*}

¹Howard Hughes Medical Institute and Department of Microbiology and Immunology, University of California, San Francisco, San Francisco, CA 94143, USA

²Department of Biochemistry and Biophysics, University of California, San Francisco, San Francisco, CA 94143, USA

³Lead contact

*Correspondence: marco.degiovanni@ucsf.edu (M.D.G.), jason.cyster@ucsf.edu (J.G.C.)

<https://doi.org/10.1016/j.immuni.2023.05.006>

SUMMARY

Cryptococcus neoformans is the leading cause of fungal meningitis and is characterized by pathogenic eosinophil accumulation in the context of type-2 inflammation. The chemoattractant receptor GPR35 is expressed by granulocytes and promotes their migration to the inflammatory mediator 5-hydroxyindoleacetic acid (5-HIAA), a serotonin metabolite. Given the inflammatory nature of cryptococcal infection, we examined the role of GPR35 in the circuitry underlying cell recruitment to the lung. GPR35 deficiency dampened eosinophil recruitment and fungal growth, whereas overexpression promoted eosinophil homing to airways and fungal replication. Activated platelets and mast cells were the sources of GPR35 ligand activity and pharmacological inhibition of serotonin conversion to 5-HIAA, or genetic deficiency in 5-HIAA production by platelets and mast cells resulted in more efficient clearance of *Cryptococcus*. Thus, the 5-HIAA-GPR35 axis is an eosinophil chemoattractant receptor system that modulates the clearance of a lethal fungal pathogen, with implications for the use of serotonin metabolism inhibitors in the treatment of fungal infections.

INTRODUCTION

Fungal pathogens have been described as “the next deadly plague.” They are responsible for 75,000 hospitalizations in the US each year. An estimated 300 million people are infected with fungal disease worldwide with 2.3 million deaths every year, a number comparable to deaths from Tuberculosis and Malaria.^{1,2} The lack of effective diagnostics, therapies, and vaccines is largely responsible for the high mortality.³ *C. neoformans*, a common cause of lethal meningitis in immunocompromised patients, is responsible for ~200,000 deaths annually worldwide, mostly in the AIDS population.^{1,4} The infectious process begins when the host inhales desiccated cryptococcal yeast or spores. Some particles find their way into the alveoli where the resident cells of the innate immune system respond to invading pathogens.⁵ While the majority of infections are asymptomatic and limited to the lungs, in immunocompromised patients *C. neoformans* may enter the circulation, leading to disseminated disease, including meningoencephalitis, which is uniformly lethal in the absence of treatment.⁴

Resistance against *C. neoformans* primarily involves immune effector mechanisms and T helper (Th) cells are key players.^{6–8} Whereas IL-12-dependent Th1 responses are protective,^{6,7,9} Th2 cells producing IL-4, IL-13, and IL-5 are detrimental to protection.^{10–14} Pulmonary eosinophilia is a common manifesta-

tion of the host response during fungal infection, but it is generally associated with non-protective Th2 immunity.^{11,14–17} Indeed, susceptible C57BL/6 mice have many eosinophils in their lungs, moderately resistant BALB/c mice have transient influx of eosinophils, and highly resistant CBA/J mice show only a few eosinophils in their lungs.¹¹ Eosinophils store preformed IL-4 within intracellular granules that are rapidly secreted upon cell activation,¹⁸ and eosinophil-derived IL-4 contributes to the development of Th2 cells in allergic disorders¹⁹ and fungal infections.^{14,15,17,20} In accordance with these observations, one study found that eosinophil-deficient mice are resistant to *C. neoformans* infection and show reduced Th2 responses.¹⁴

The receptor CCR3 and its eotaxin ligands play a critical role in eosinophil recruitment to the lung in allergy models,^{21–23} but their role during fungal infections remains to be clarified. Platelets^{24,25} and mast cells^{2,5} are activated upon cryptococcal infection and communicate with eosinophils to sustain their activation, recruitment and survival through the production of several mediators including eotaxin(s).^{26,27} However, reductions or increases in recruited eosinophils do not necessarily correlate with differences in eotaxin levels,^{16,28} suggesting that other mechanisms could shape eosinophil recruitment in some contexts. Thus, despite the strong evidence that eosinophils have a detrimental effect on clearance of *Cryptococcus* from the lungs, the mechanisms

responsible for eosinophil recruitment to the infected lung are not well understood.

The G-protein-coupled receptor GPR35 is widely expressed by myeloid cells in humans and mice. In recent work, we established that the serotonin metabolite 5-hydroxyindoleacetic acid (5-HIAA) functions as a physiological GPR35 ligand.²⁹ Expression of *Gpr35* is increased in activated neutrophils and the 5-HIAA-GPR35 ligand-receptor system contributes to recruitment of neutrophils to the inflamed peritoneum and skin.²⁹ Platelets and mast cells were identified as important sources of 5-HIAA in these inflamed tissues. Work *in vitro* and in zebrafish has suggested that GPR35 may also function as chemoattractant or adhesion-promoting receptor in monocytes and macrophages,³⁰ but how widely this is the case and whether GPR35 functions as a recruitment receptor in other myeloid cell types is not clear. Moreover, given the multiple and often distinct sets of chemoattractants induced under different inflammatory conditions and in different tissues, it is currently difficult to predict which chemoattractants will be most important in a given disease setting.

Here, we examined the impact of GPR35 in the response to pulmonary *C. neoformans* infection. GPR35 was highly expressed in activated eosinophils and expression in eosinophils contributed to their entry to the infected lung and thereby to type 2-skewing of the effector T cell response and less efficient fungal clearance. 5-HIAA production by platelets and mast cells promoted eosinophil recruitment from blood vessels into the lung parenchyma. Our findings identify 5-HIAA and GPR35 as a chemoattractant receptor system acting on eosinophils to promote their recruitment to the lungs and demonstrate the contribution of this recruitment system to fungal pathogenesis.

RESULTS

GPR35 expression in bone marrow-derived cells supports eosinophil recruitment and fungal infection

To test whether GPR35 has a role in the immune response to respiratory *C. neoformans* infection, *Gpr35*^{+/-} and *Gpr35*^{-/-} mice were infected intranasally with 1×10^5 colony-forming units (CFUs) of the KN99 strain. Measurements of lung and spleen fungal CFU 11 days later revealed a significant protective effect of GPR35-deficiency (Figures 1A and 1B). Histological analysis showed that *GPR35*^{-/-} mice had reduced lung pathology (Figures S1A and S1B). GPR35 is expressed by a range of non-hematopoietic as well as hematopoietic cells.^{29,31-34} To determine if the susceptibility-promoting effect of GPR35 reflected action in hematopoietic cells, irradiated WT mice that had been reconstituted with *GPR35*^{+/-} or *GPR35*^{-/-} bone marrow (BM) were intranasally infected with *C. neoformans*. Again, GPR35-deficiency was associated with a lower fungal burden (Figures 1C and 1D). These data indicate that GPR35 in a hematopoietic cell type negatively impacts the ability to clear *Cryptococci* from the lung, resulting in increased systemic spread of the pathogen. Analysis of inflammatory cell accumulation in the inflamed lung revealed few neutrophils were present on day 11 as expected and these were unaffected by GPR35-deficiency (Figure S1C). Flow cytometric analysis showed GPR35 was minimally expressed in neutrophils from infected mice (Figure S1D). Monocyte and alveolar macrophage fre-

quencies were similarly unaffected by GPR35-deficiency (Figures S1E and S1F). In contrast, eosinophil frequencies and numbers were significantly reduced in the lungs of infected *GPR35*^{-/-} mice (Figures 1E–1H). Eosinophil frequencies in BM and blood at steady state were unaltered by GPR35-deficiency (Figures S1G and S1H). Since it was possible that the reduced lung eosinophil number was secondary to the reduced CFU burden at day 11 we next examined mice at an earlier time point after infection. At day 4 post-infection, lung fungal burden in WT and *GPR35*^{-/-} mice was similar but eosinophils counts were significantly lower in *GPR35*^{-/-} mice (Figures 1I and 1J). Analysis of neutrophil recruitment at an early time point showed it was not significantly altered by GPR35 deficiency (Figure S1I). Thus, GPR35 deficiency led to less eosinophil accumulation in the lung prior to any effect on lung fungal burden.

Requirement for GPR35 in eosinophils

To test whether GPR35 was required intrinsically in eosinophils for their accumulation in the lung we generated and infected *GPR35*^{-/-} + WT (~1:1) mixed BM chimeras. Analysis at day 4 and 11 post-infection revealed a selective deficiency in *GPR35*^{-/-} eosinophil recruitment in the lung (Figures 2A, 2B, S1J, and S1K). Hematopoietic chimerism in the reconstituted mice was determined using B cells since this cell lineage has not been found to express GPR35. As a further approach to test the eosinophil intrinsic requirement of GPR35, we used an *in vitro* BM culture system to generate WT and *GPR35*^{-/-} eosinophils.³⁵ 1 day after transfer into mice previously infected for 5 days, we observed a significant deficit in *GPR35*^{-/-} eosinophil recruitment to the infected lung (Figures 2C and 2D). By *in vivo* antibody pulse-labeling of blood-exposed cells,³⁶ we found increased percentages of intravascular *GPR35*-deficient compared with WT eosinophils indicating less efficient extravasation into the lung parenchyma (Figures 2E and 2F).

Using an antibody specific for the GPR35 C terminus and intracellular staining, GPR35 could be detected in eosinophils from the infected lung (Figure 2G) but not in eosinophils from the BM of control mice (Figure S1L). Using a transwell migration assay, we found that *GPR35*^{+/+} but not *GPR35*^{-/-} eosinophils from lungs of *C. neoformans* infected mice migrated to low nanomolar concentrations of 5-HIAA (Figure 2H). WT and *GPR35*^{-/-} cells were similar in their migratory responses to CCL11 (eotaxin-1) and CXCL12 (Figure S1M). Eosinophil migration to 5-HIAA was inhibited by pretreatment with pertussis toxin, consistent with GPR35 signaling in these cells involving G α i-containing heterotrimeric G-proteins (Figure S1N). These findings demonstrate that GPR35 acts in activated eosinophils to promote their migration toward 5-HIAA and their accumulation in the infected lung.

GPR35 overexpression augments *Cryptococcus* accumulation and eosinophil recruitment

The above findings indicated that GPR35 is necessary for augmenting *C. neoformans* infection and for promoting eosinophil recruitment. To ask whether the receptor is sufficient to have these effects, we generated chimeras using BM cells that had been transduced with a GPR35-eGFP encoding or control retroviral construct. The efficiency of reconstitution with transduced (eGFP reporter-expressing) hematopoietic cells was similar for

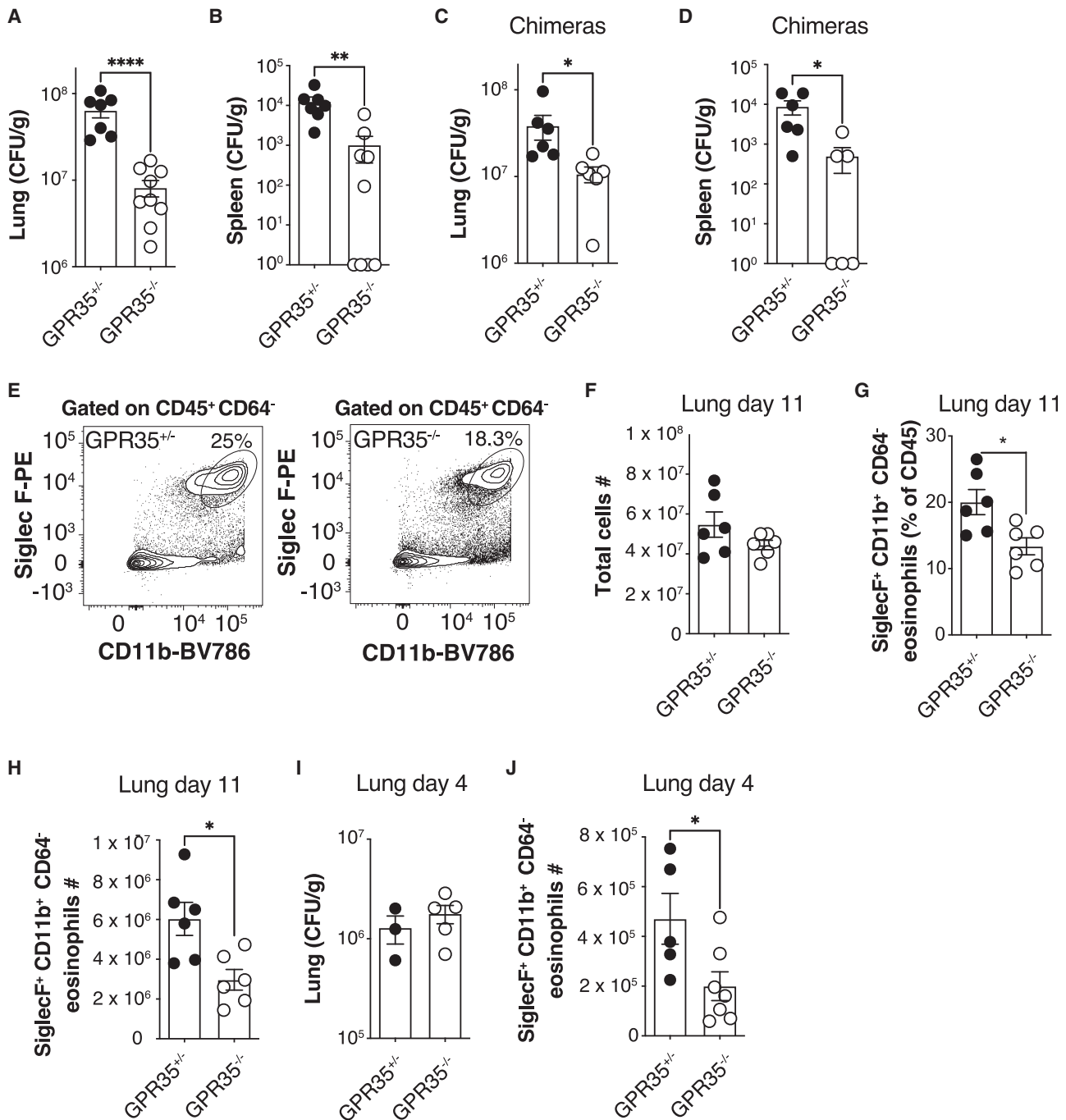


Figure 1. GPR35 in BM-derived cells promotes increased *Cryptococcus* burden and eosinophil recruitment to the infected lung

(A–D) Quantification of *C. neoformans* CFUs in lung and spleen of GPR35^{+/+} and GPR35^{-/-} mice (A and B) or full chimeras (C and D) 11 days after intranasal infection. (A and B), n = 7–9; (C and D), n = 6. Data are pooled from two independent experiments.

(E) Flow cytometry plots showing percentages of SiglecF⁺ CD11b⁺ eosinophils in GPR35^{+/+} (left) and GPR35^{-/-} (right) out of CD45⁺ CD64⁻ cells in the lung.

(F–H) Quantification of total cell numbers (F), SiglecF⁺ CD11b⁺ CD64⁻ eosinophil percentages out of CD45⁺ cells, (G) and numbers (H) in the lung of GPR35^{+/+} and GPR35^{-/-} full chimeras 11 days after intranasal infection. n = 6. Data are pooled from two independent experiments.

(I and J) Quantification of *C. neoformans* CFUs (I) and SiglecF⁺ CD11b⁺ CD64⁻ eosinophil numbers (J) in lungs of GPR35^{+/+} and GPR35^{-/-} mice 4 days after intranasal infection. (F–H), n = 6; (I), n = 3–5; (J) = 5–7. Data are pooled from two independent experiments. *p < 0.05; **p < 0.005; ****p < 0.0001. Data are presented as mean ± SEM. See also Figure S1.

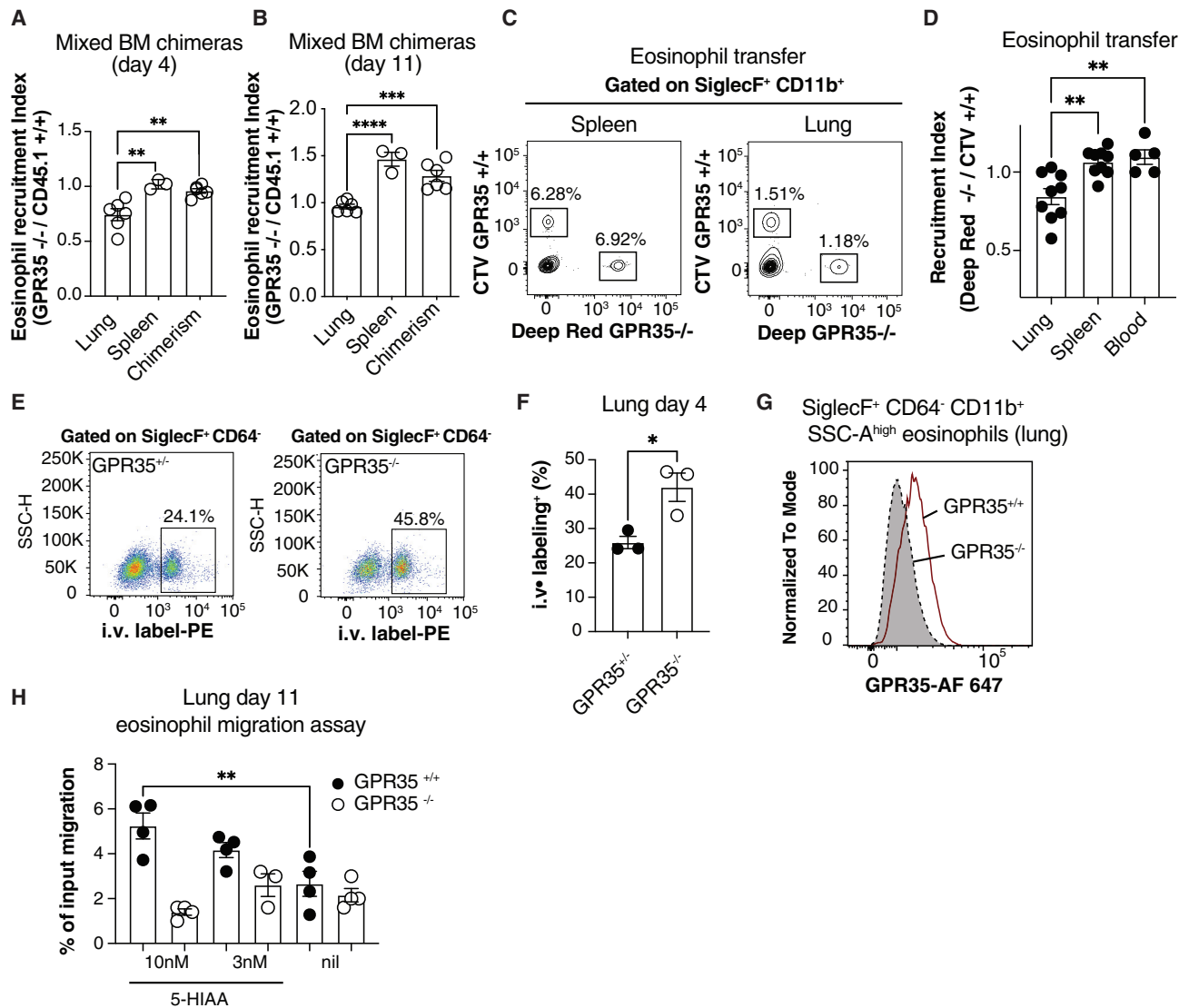


Figure 2. Intrinsic requirement for GPR35 in eosinophils

(A and B) Quantification of eosinophil recruitment index in lung and spleen of *C. neoformans* infected CD45.2⁺ GPR35^{-/-} + CD45.1⁺ GPR35^{+/+} mixed chimeras, 4 (A) or 11 (B) days after intranasal infection. The chimerism was calculated as the CD45.2⁺/CD45.1⁺ ratio within blood B220⁺ cells at the time of tissue isolation. n = 3–6. Data are pooled from two independent experiments.

(C) Flow cytometry plots showing transferred CTV⁺ GPR35^{+/+} and Deep Red⁺ GPR35^{-/-} BM-derived eosinophils in spleen and lung of mice infected 5 days before with *C. neoformans*, 24 h after cell injection.

(D) Quantification of transferred eosinophils determined as in (C), shown as recruitment index in lung, spleen, and blood of infected mice, 24 h after cell transfer. n = 5–9. Data are pooled from three independent experiments.

(E and F) Flow cytometry plots (E) and quantification (F) of 2 min intravascular labeled (i.v. CD45-PE⁺) SiglecF⁺ CD64⁻ eosinophils in lungs of GPR35^{+/-} (left) and GPR35^{-/-} (right) mice 4 days after *C. neoformans* infection. n = 3. Data are representative of two independent experiments.

(G) Flow cytometry plot showing GPR35 expression in GPR35^{+/-} and GPR35^{-/-} SiglecF⁺ CD11b⁺ CD64⁻ eosinophils in the lungs 11 days after intranasal infection. Data are representative of at least 2 independent experiments.

(H) Transwell migration assay to 5-HIAA (nM) of GPR35^{+/-} and GPR35^{-/-} eosinophils isolated from *C. neoformans* infected lung 11 days after infection. Nil indicates no added chemoattractant. n = 3–4. Data are representative of three independent experiments. *p < 0.05; **p < 0.005; ***p < 0.0005; ****p < 0.0001. Data are presented as mean ± SEM. See also [Figure S1](#).

recipients receiving either construct (Figure S2). Analysis of the BM chimeras 9 and 11 days after *C. neoformans* infection revealed a higher fungal burden in the GPR35-overexpressing mice (Figures 3A and 3B), and a strong enrichment for GPR35 overexpressing eosinophils in the lungs (Figures 3C–3E). Thus,

while the retroviral transduction system does not allow us to restrict the increased GPR35 expression to eosinophils, the findings to this point indicate that GPR35 expression is both necessary and limiting for tissue fungal burden and eosinophil accumulation.

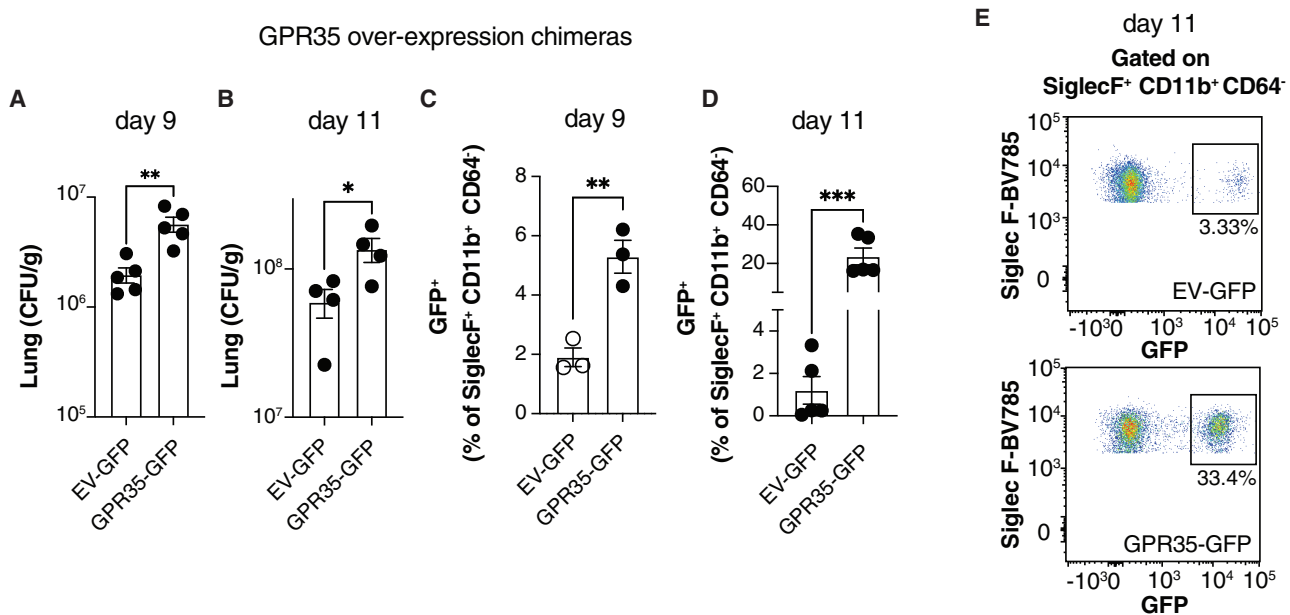


Figure 3. GPR35 overexpression augments *Cryptococcus* infection and eosinophil recruitment

(A–D) Quantification of *C. neoformans* CFUs (A and B) and GFP⁺ eosinophil percentages (C and D) in empty vector (EV)-GFP or GPR35-GFP overexpressing chimeras, 9 (A and C) or 11 (B and D) days after intranasal infection. (A, B, and D), n = 4–5; (C), n = 3.

(E) Flow cytometry plots showing GFP⁺ percentages within SiglecF⁺ CD11b⁺ CD64⁻ eosinophils quantified in (D). Data are pooled (A) or representative (B–D) of two independent experiments. *p < 0.05; **p < 0.005; ***p < 0.0005. Data are presented as mean ± SEM. See also Figure S2.

GPR35 expressing eosinophils sustain *Cryptococcus* infection

The transcription factor GATA1 is critical for eosinophil differentiation and mice with a mutation in the GATA1 promoter (referred to as Δ dblGATA1) have a selective deficiency in eosinophils.^{37,38} To test the importance of eosinophil GPR35 expression in promoting *C. neoformans* infection of the lung we generated GPR35^{-/-} + Δ dblGATA1 (1:1) mixed BM chimeras. In these mice, all the eosinophils lack GPR35 whereas all other hematopoietic lineages are ~50% derived from WT BM. Analysis of the BM chimeras at day 11 post-infection showed that selective GPR35 deficiency in eosinophils led to a similar reduction in lung CFU as in mice fully deficient in hematopoietic GPR35 (Figure 4A). These chimeras were also used to confirm the intrinsic role of GPR35 in eosinophil recruitment to the lung and the block in eosinophil development in full GATA1-deficient BM chimeras (Figure 4B). Notably, eosinophil-deficient Δ dblGATA1 BM chimeras had a similar reduction in lung CFU as mice lacking GPR35 in eosinophils (Figure 4A) suggesting GPR35 is critical for the disease-promoting activity of the eosinophils in this infection. We also tested for a possible role of GPR35 in dendritic cells (DCs) by generating mixed CD11c-DTR + GPR35^{-/-} mixed BM chimeras and treating with diphtheria toxin (DT) prior to *C. neoformans* infection. GPR35-deficiency in DCs (and other cells sensitive to CD11c-DTR mediated ablation) did not alter the susceptibility to lung *C. neoformans* infection (Figures S3A and S3B).

Increased lung Th1 response in the absence of GPR35

Previous studies have established that eosinophils amplify the generation of IL-4-producing T cells in the *C. neoformans* in-

fecting lung, a polarizing activity that is associated with less effective fungal clearance.^{14,15,17,20} To determine whether the reduced eosinophil recruitment caused by GPR35 deficiency led to an altered polarization of the T cell response, we examined the properties of effector CD4 T cells in the lungs at day 11. Infected GPR35-deficient mice had an increase in IFN γ cytokine expression by CD4 T cells and an increased frequency of Tbet⁺ cells (Figures 4C–4E and S4A). Importantly, the frequency of IL-4-expressing CD4 T cells was significantly reduced (Figures 4F and S4A). The frequency of GATA3⁺ T cells was unchanged (Figure 4G), suggesting that GATA3⁺ Th2 cell generation in lymph nodes was unaffected and that eosinophils promoted upregulation of IL-4 expression in effector CD4 T cells in the lung. To determine whether the action of GPR35 in promoting Th2 responses was within eosinophils we generated 1:1 mixed GPR35^{-/-} + Δ dblGATA1 BM chimeras. At day 11 after infection, lung CD4 T cells in GPR35^{-/-} + Δ dblGATA1 BM chimeras showed less expression of IL-4 and increased IFN γ (Figures 4H and 4I), and there was an increase in the frequency of Tbet⁺ T cells (Figure 4J). These findings establish the importance of GPR35-mediated eosinophil recruitment in favoring a Th2 effector response in the lung.

5-HIAA is required for GPR35-mediated eosinophil recruitment to the infected lung

The GPR35 ligand 5-HIAA was strongly upregulated in the lungs at days 4 and 11 after infection (Figure 5A). To test the importance of 5-HIAA in eosinophil recruitment to the *C. neoformans* infected lung, mice were treated with phenelzine, a monoamine oxidase (MAO) inhibitor that prevents serotonin metabolism to

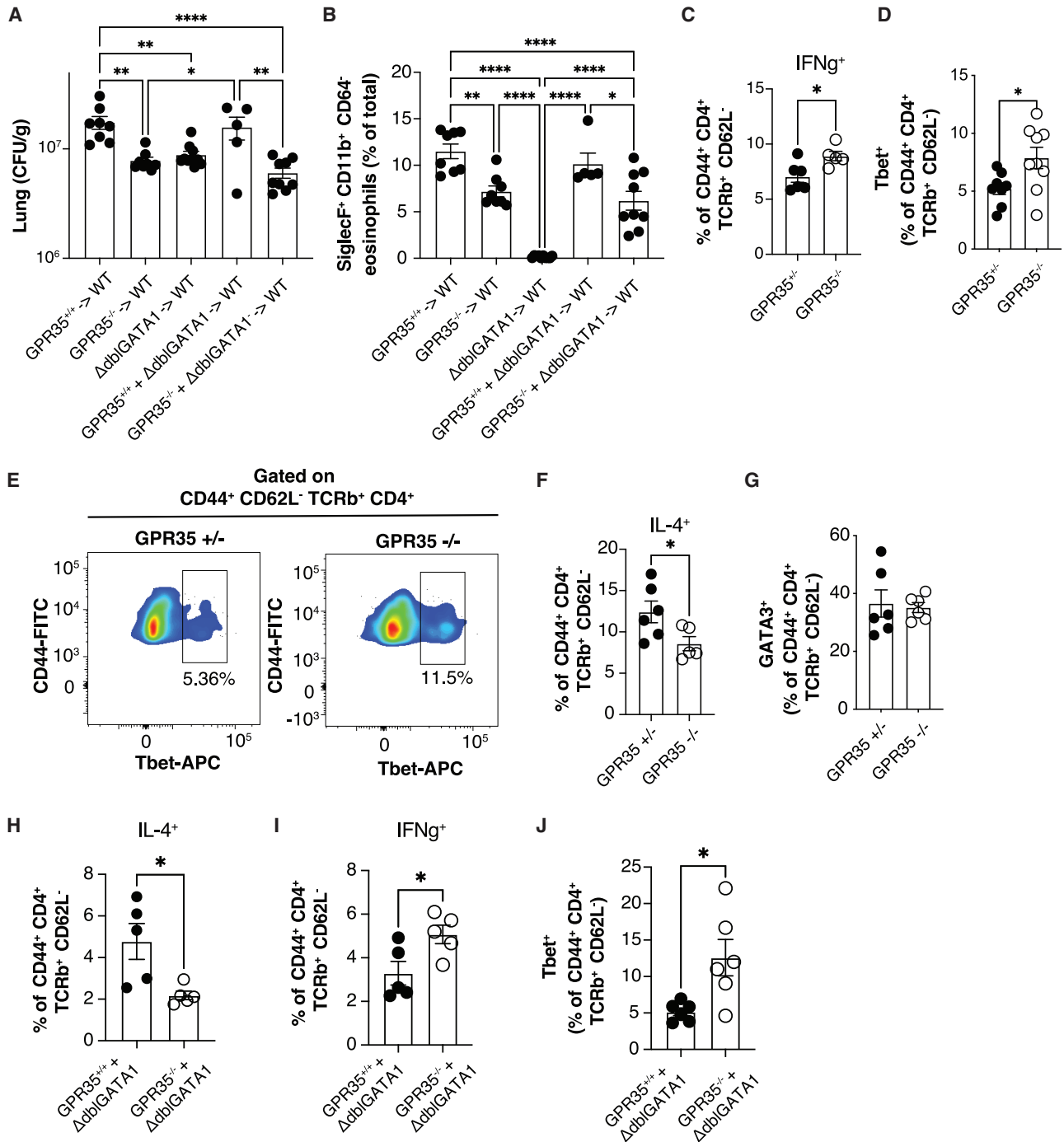


Figure 4. GPR35 expressing eosinophils sustain *Cryptococcus* infection

(A and B) Quantification of *C. neoformans* CFUs (A) and SiglecF⁺ CD11b⁺ CD64⁻ eosinophil percentages (B) in the lung of the indicated full and mixed BM chimeras 11 days after intranasal infection. n = 5–10. Data are pooled from two independent experiments.

(C and D) Quantification of *ex vivo* stimulated IFNγ⁺ cells (C) and Tbet⁺ Th1 cell percentages (D) out of CD4⁺ CD44⁺ TCRβ⁺ CD62L⁻ in the lung of GPR35^{+/+} and GPR35^{-/-} full chimeras 11 days after intranasal infection. (C), n = 5–6; (D), n = 8–9. Data are pooled from three (C) or two (D) independent experiments.

(E) Flow cytometry plot showing Tbet⁺ Th1 percentages in GPR35^{+/-} (left) and GPR35^{-/-} (right) infected mice quantified in (D).

(F and G) Quantification of *ex vivo* stimulated IL-4⁺ cell percentages (F) and GATA3⁺ Th2 cell percentages (G) out of CD4⁺ CD44⁺ TCRβ⁺ CD62L⁻ cells in the lung of GPR35^{+/+} and GPR35^{-/-} mice 11 days after intranasal infection. n = 5–6.

(H–J) Quantification of *ex vivo* stimulated IL-4⁺ (H), IFNγ⁺ (I), and Tbet⁺ (J) cells out of CD4⁺ CD44⁺ TCRβ⁺ CD62L⁻ cells in the lung of GPR35^{-/-} + ΔdblGATA1 and control mixed BM chimeras, 11 days after intranasal infection. n = 5–6. Data are pooled from two independent experiments. *p < 0.05; **p < 0.005; ****p < 0.0001. Data are presented as mean ± SEM. See also Figures S3 and S4.

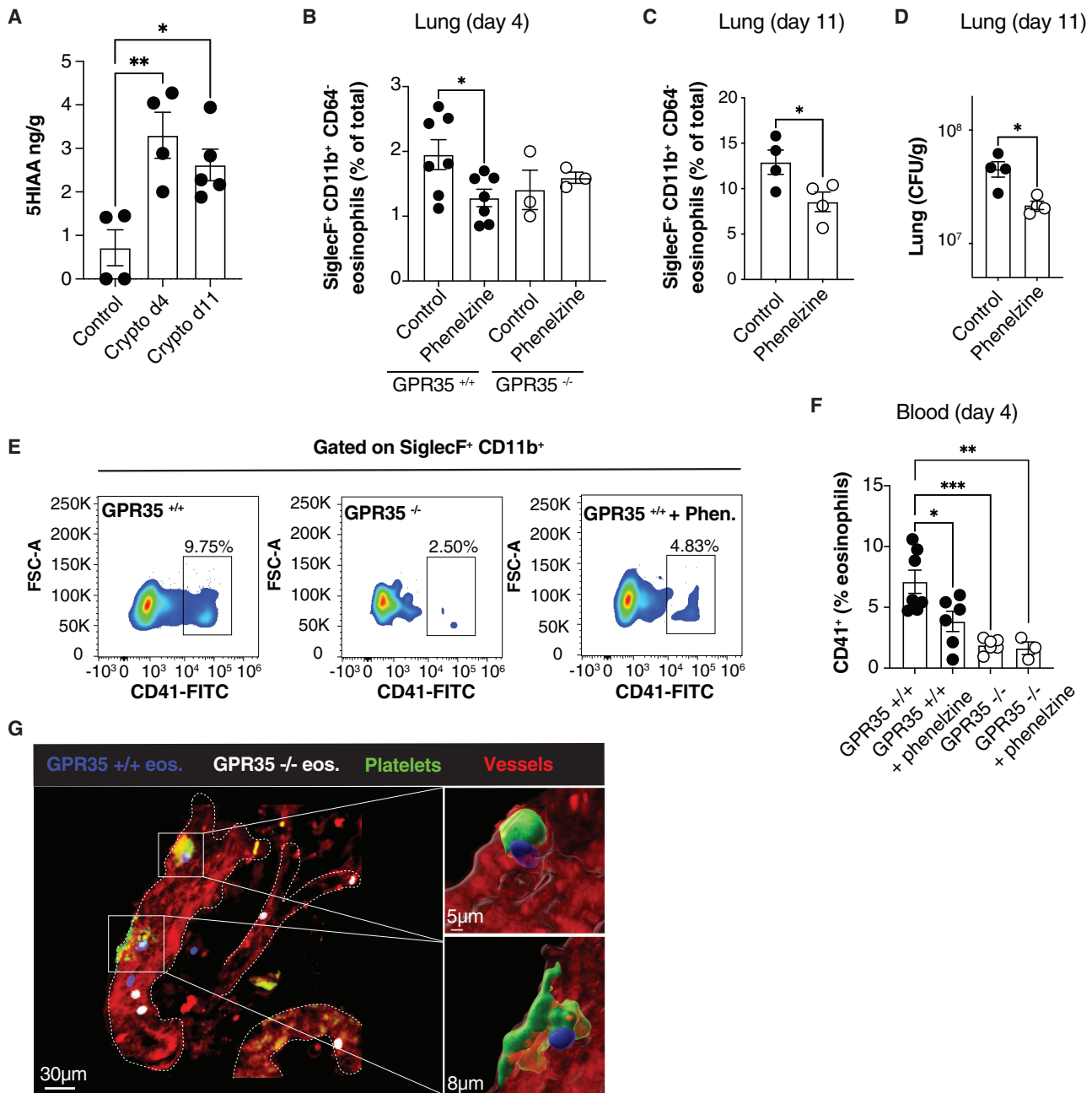


Figure 5. 5-HIAA is required for GPR35-mediated eosinophil recruitment to the infected lung

(A) Quantification by ELISA of 5-HIAA concentrations in the lung of uninfected mice or *C. neoformans* infected mice (4 or 11 days after infection). $n = 4-5$. Data are pooled from two independent experiments.

(B–D) Quantification of SiglecF⁺ CD11b⁺ CD64⁻ eosinophil percentages (B and C) and *C. neoformans* CFUs (D) in the lung of GPR35^{+/+} and GPR35^{-/-} mice not treated or treated with phenelzine, 4 (B) or 11 (C and D) days after intranasal infection. (B), $n = 3-7$; (C and D), $n = 4$. Data are pooled from two independent experiments.

(E and F) Flow cytometry plots (E) and quantification (F) of CD41⁺ SiglecF⁺ CD64⁻ eosinophils in the blood of not treated or phenelzine-treated GPR35^{+/+} and GPR35^{-/-} mice, 4 days after intranasal infection. $n = 3-7$. Data are pooled from two independent experiments.

(G) Multiphoton micrograph of *C. neoformans* infected lung from platelet-reporter mice (P14-Cre x mTmG mice), 4 days after intranasal infection. Transferred BM-derived GPR35^{+/+} (CTV⁺, blue) and GPR35^{-/-} (Deep Red⁺, white) eosinophils, and endogenous platelets (green) and vessels (red) are shown. Data are representative of at least two independent experiments. * $p < 0.05$; ** $p < 0.005$; *** $p < 0.0005$. Data are presented as mean \pm SEM.

5-HIAA,^{29,39} starting 3 days before infection. Phenelzine treatment led to a reduction in WT but not GPR35-deficient eosinophil recruitment at day 4 post-infection (Figure 5B). Phenelzine treatment also reduced eosinophil numbers in the lung at day 11 and lowered lung fungal burden (Figures 5C and 5D). ELISA analysis confirmed that lung 5-HIAA abundance was significantly reduced by the treatment (Figure S4B).

Activated platelets are a source of 5-HIAA and previous work has shown that platelets can contribute to eosinophil recruitment to sites of inflammation.^{40,41} As a measure of the extent of intravascular platelet-eosinophil interaction following infection, we assessed eosinophil acquisition of the platelet marker CD41.^{29,42} Compared with infected WT mice there was an approximately 4-fold reduction in the frequency of CD41⁺ eosinophils in infected GPR35^{-/-} mice (Figures 5E and 5F). Phenelzine treatment also led to a reduction in the CD41⁺ eosinophil frequency in WT mice (Figures 5E and 5F). In accord with phenelzine acting by reducing GPR35 ligand production, the drug had no effect on the frequency of CD41⁺ eosinophils in GPR35-deficient mice (Figure 5F).

To examine the impact of GPR35 on tissue eosinophils and platelet interactions, we performed multiphoton imaging of lung from day 4 infected mTmG PF4-Cre mice that (1) harbor GFP⁺ platelets and have strong tdTom expression in endothelium, and (2) received a mixture of WT and GPR35^{-/-} BM-derived eosinophils 6 h earlier. These studies revealed examples of WT eosinophils (blue) interacting with platelet clusters (Figure 5G; Videos S1 and S2) while GPR35^{-/-} eosinophils (white) in the same vessels showed less association with the platelet clusters (Figure 5G; Videos S1 and S2).

To quantitatively assess the contribution of platelets and mast cells to eosinophil recruitment, we infected mice lacking either of these cell types. At day 4 post-infection both platelet-deficient mice and mast cell-deficient mice showed reduced eosinophil recruitment in lungs and a higher fraction of eosinophils within the blood, similarly to GPR35^{-/-} mice (Figures 6A–6C). These data are consistent with platelets and mast cells augmenting the post-attachment transendothelial migration step. In addition, reduced eosinophil recruitment correlated with a reduction in CFUs at day 11 in the absence of platelets or mast cells (Figure 6D). Furthermore, GPR35 influence on eosinophil recruitment was lost in the absence of platelets or mast cells (Figures 6E and 6F), consistent with the conclusion that platelet- and mast-cell-derived 5-HIAA sustains eosinophil recruitment to infected lungs. ELISA analysis confirmed that lung 5-HIAA abundance was significantly reduced by platelet deficiency and mast cell deficiency (Figure S4C).

The serotonin transporter (SERT) is important for platelets to acquire serotonin, and thus SERT^{-/-} mice lack MAO-generated 5-HIAA in their platelets.⁴³ At day 4 post-infection SERT^{-/-} mice showed a similar reduction in lung eosinophils to GPR35-deficient and platelet-deficient mice (Figure 6A), and they reciprocally showed a similar increase in blood eosinophils (Figure 6B). At day 11, SERT^{-/-} mice continued to show lower lung eosinophils (Figure S4D) and CFUs were reduced (Figure S4E). In contrast to platelets, mast cells express tryptophan hydroxylase-1 (Tph1) enabling them to synthesize serotonin from tryptophan; they also express MAO (Immgen.org) and convert serotonin to 5-HIAA.^{29,44–47} Mast cells are the main Tph1⁺ hematopoietic cell

type (Immgen.org). In WT mice that had been reconstituted with Tph1-deficient BM such that their mast cells lacked the ability to generate 5-HIAA, there was less efficient eosinophil recruitment to the *C. neoformans* infected lung and reduced fungal CFUs (Figures 6G and 6H). To test the importance of 5-HIAA generation in mast cells more definitively, we crossed Tph1 floxed mice with Cpa3-Cre mice that express Cre selectively in mast cells and a fraction of basophils.⁴⁸ Analysis of Tph1^{fl/fl} Cpa3-Cre mice at day 11 after *C. neoformans* infection showed the mice had fewer lung eosinophils (Figures 6I and 6J) and a lower lung fungal burden (Figure 6K). Taken together, these findings are consistent with platelets and mast cells cooperating in promoting GPR35⁺ eosinophil recruitment to the infected lung through production of 5-HIAA.

DISCUSSION

Precise, selective control of immune cell recruitment is critical for determining the outcome of inflammation. Here, we present evidence that 5-HIAA is a novel driver of eosinophil recruitment to the lung during the initial pulmonary phase of cryptococcal infection. We propose a model whereby fungal infection causes lung platelet and mast cell activation and release of 5-HIAA. GPR35^{hi} eosinophils that have attached to lung blood vessels encounter the 5-HIAA and it cooperates with other locally produced factors to augment eosinophil adhesion in association with platelet clusters. 5-HIAA emanating from perivascular mast cells then helps promote eosinophil extravasation into the tissue. We present findings with GPR35-deficient and over-expressing eosinophils, platelet-, and mast-cell-deficient mice, and mice unable to generate 5-HIAA in platelets or mast cells, that support this model. Furthermore, we show that GPR35 deficiency causes a shift toward a type I immune response and improved fungal clearance. Tissue eosinophils produce mediators, including IL-4, that contribute to type II skewing of the immune response. It has been speculated⁴⁹ that *C. neoformans* evolved to promote a type II immune response as a mechanism of evading the type I response that is more effective at killing intracellular organisms. We suggest that by augmenting eosinophil recruitment to the lung, 5-HIAA and GPR35 favor a type II immune response and thus contribute to the *C. neoformans* immune evasion mechanism. An implication of these findings is that agents that reduce 5-HIAA or antagonize GPR35 might have therapeutic benefit in *C. neoformans* infections.

Previous work established a role for GPR35 and 5-HIAA in neutrophil recruitment to the inflamed peritoneum and inflamed skin and lymph nodes.²⁹ The lack of an effect of GPR35 deficiency on neutrophil recruitment to the *C. neoformans* infected lung may reflect a lack of GPR35 induction on neutrophils during cryptococcal infection and possible redundancy with other inflammation-induced neutrophil chemoattractants. Multiple chemoattractants have also been defined for eosinophils, including eotaxins (CCL11, CCL24, and CCL26), CCL5, CXCL12, prostaglandins, and oxysterols.^{27,50} It is thus striking that GPR35 makes a non-redundant contribution to eosinophil recruitment to the *Cryptococcus* infected lung. It will be important in future work to define the signals promoting GPR35 upregulation in activated eosinophils and to examine the contribution of 5-HIAA to their recruitment during different inflammatory insults in the lung and other tissues.

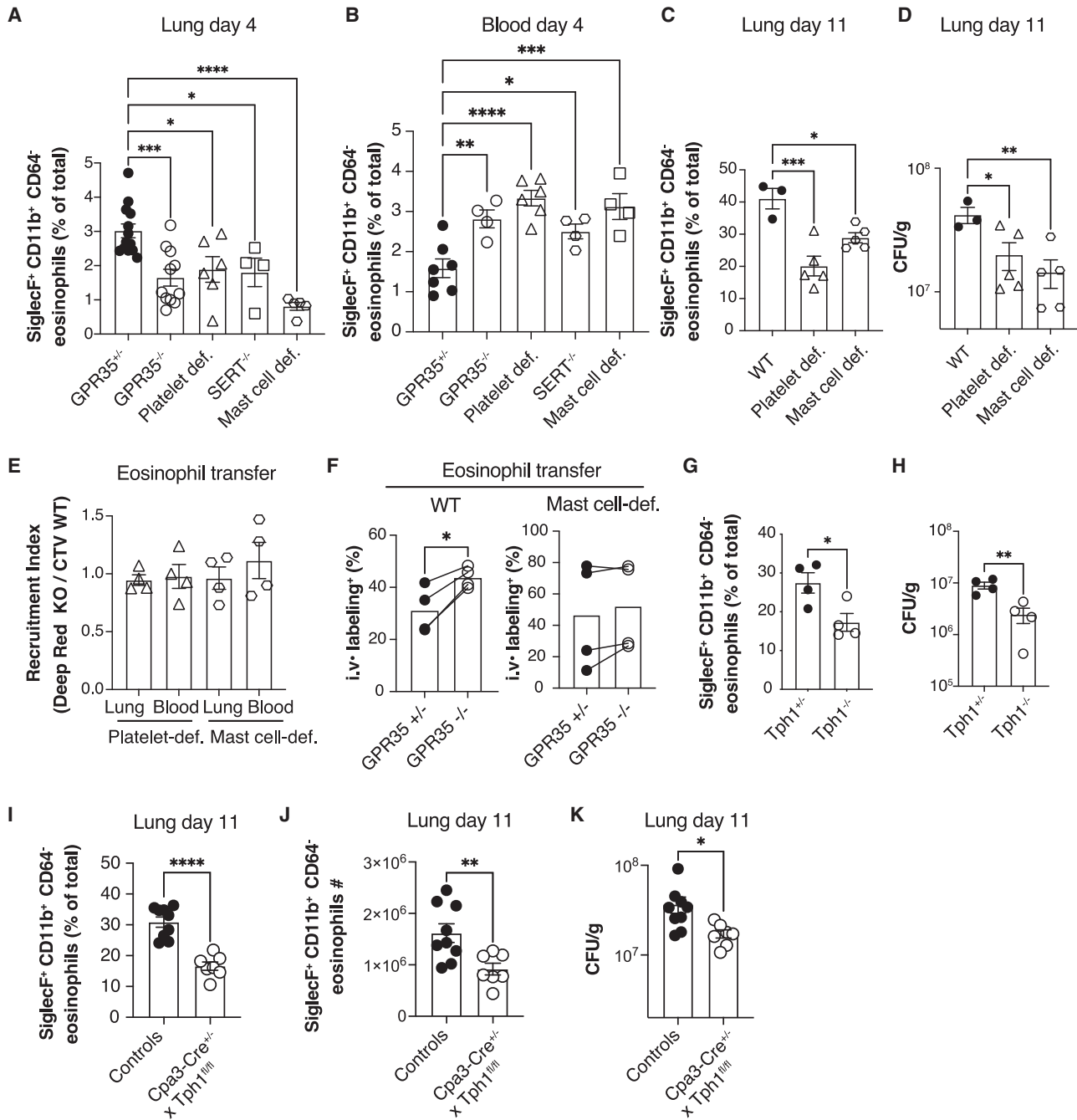


Figure 6. Platelets and mast cells are required for GPR35-mediated eosinophil recruitment to the infected lung

(A and B) Quantification of SiglecF⁺ CD11b⁺ CD64⁻ eosinophil percentages in lungs (A) and blood (B) of *C. neoformans* infected GPR35^{+/+}, GPR35^{-/-}, platelet-deficient (*cmlp*^{-/-}), SERT^{-/-} and mast-cell-deficient (*Kit*^{W/W}) mice, 4 days after intranasal injection. (A), n = 4–13; (B), n = 4–7.

(C and D) Quantification of SiglecF⁺ CD11b⁺ CD64⁻ eosinophil percentages (C) and *Cryptococcus* CFUs (D) in the lung of WT, platelet-deficient or mast cell-deficient mice, 11 days after intranasal infection. n = 3–5. Data are pooled from two independent experiments.

(E and F) Quantification of transferred BM-derived CTV⁺ GPR35^{+/+} and Deep Red⁺ GPR35^{-/-} eosinophil recruitment index (E) and intravascular labeling (F), in the lung and blood of *C. neoformans* infected (day 5) WT, platelet-deficient and/or mast cell-deficient mice, 24 h after cell transfer. n = 4.

(G and H) Quantification of SiglecF⁺ CD11b⁺ CD64⁻ eosinophil percentages (G) and *C. neoformans* CFUs (H) in the lung of Tph1^{+/+} and Tph1^{-/-} full BM chimeras, 11 days after intranasal infection. n = 4.

(I–K) Quantification of SiglecF⁺ CD11b⁺ CD64⁻ eosinophil percentages (I), absolute numbers (J), or *Cryptococcus* CFUs in the lung (K) of Cpa3-Cre⁺ x Tph1^{fl/fl} mice and littermate controls (Cpa3-Cre⁺ Tph1^{fl/wt} and Cpa3-Cre⁺ x Tph1^{fl/fl}) 11 days after intranasal infection. n = 7–9. *p < 0.05; **p < 0.005; ***p < 0.0005, ****p < 0.0001. Data are pooled from at least two independent experiments. Data are presented as mean ± SEM.

Platelets have a well-established role in augmenting neutrophil attachment to and transmigration across inflamed endothelium.⁵¹ Several studies have also shown platelets promoting eosinophil accumulation in inflamed tissues, including the lung.^{40,41} Multiple platelet-derived factors are likely to be involved in engaging eosinophils, including P-selectin, integrin α IIbB3, platelet factor-4 (PF4), CCL5, and platelet activating factor (PAF).^{27,40,41} We suggest that 5-HIAA cooperates with other platelet-derived factors to promote eosinophil adhesive interactions with endothelium-attached activated platelet clusters. This attachment is expected to augment subsequent transendothelial migration. In accord with our imaging and functional data, activated platelets in the lung vasculature have been observed in several inflammatory conditions⁴⁰ including in the lungs of COVID-19 patients.⁵² Our finding of a new platelet-derived mediator contributing to eosinophil recruitment to the lung highlights the diverse roles of platelets in shaping the lung inflammatory cell recruitment process during infection.

Perivascular mast cells are numerous in the lung and skin.^{53–57} The stimuli promoting mast cell activation during fungal infection are not well studied but may include β -glucans and ligands for TLR4 and CCR1.^{3,49} Similar to platelets, mast cells release chemoattractive mediators, including PAF and CCL5, that can act on eosinophils.^{27,57} However, in contrast to their production of neutrophil-attracting chemokines, they have not yet been shown to produce the best-defined eosinophil chemoattractants, the eotaxins CCL11, CCL24, and CCL26. Mast cell mediators, including histamine and serotonin, cause changes in the endothelium that facilitate platelet and eosinophil attachment and cell transmigration. 5-HIAA is likely to cooperate with other mast-cell-derived factors in promoting eosinophil recruitment into the infected lung.

Our work was all performed in the mouse and future studies will be needed to test the function of GPR35 in human eosinophils. Possibly in accord with GPR35 contributing to cryptococcal pathogenesis in humans, a GPR35 nonsense mutation predicted to cause C terminus truncation and hypothetically increased receptor activity has been identified in a patient with non-HIV cryptococcal meningoencephalitis.⁵⁸ While GPR35 and 5-HIAA action in mouse eosinophils has an adverse effect on the response to *C. neoformans*, we anticipate that this chemoattractant receptor system will play critical roles in protection from other lung pathogens, especially in cases where eosinophils or neutrophils are required for protection. An important question that emerges from this study is whether clinically approved drugs that block serotonin uptake and thereby deplete platelets of serotonin and 5-HIAA, or that block serotonin metabolism to 5-HIAA, would have efficacy in reducing eosinophil recruitment, type II effector T cell induction and cryptococcal disease. In this regard, it is notable that a clinical study provided preliminary evidence that treatment of patients with a SERT inhibitor may be protective from *C. neoformans* disease.⁵⁹ While the mechanism has been thought to involve direct antifungal actions of this agent,^{60,61} we suggest that it may be acting by reducing 5-HIAA availability in the lung and decreasing eosinophil recruitment.

Limitations of the study

Although we used multiple approaches to modulate 5-HIAA production (phenelzine treatment, SERT^{-/-}, Tph1^{-/-} BM chimeras, Tph1^{fl/fl} Cpa3-Cre mice), each of these approaches also impacts

on serotonin production. While not a ligand for GPR35, serotonin can engage any of 14 receptors and can have pleiotropic actions in tissues.⁴³ We cannot exclude that some of the effects observed under conditions of altered 5-HIAA generation also reflect effects of altered serotonin abundance or the abundance of other serotonin metabolites or related amines. Use of a 5-HIAA catabolic enzyme to selectively deplete 5-HIAA from tissues would be a valuable approach but to our knowledge no such enzyme has been identified. In addition, while our data indicate that GPR35-expressing eosinophils modulate Th1/Th2 balance within infected airways, whether alterations of this balance are required for GPR35-mediated fungal outgrowth remains to be established. Finally, we note that performing our experiments with the widely studied *C. neoformans* KN99 strain allows our work to be placed in context with a large body of existing literature. However, we acknowledge that this is a laboratory adapted strain, and it remains important in the future to perform studies with human *C. neoformans* isolates.

STAR★METHODS

Detailed methods are provided in the online version of this paper and include the following:

- KEY RESOURCES TABLE
- RESOURCE AVAILABILITY
 - Lead contact
 - Materials availability
 - Data and code availability
- EXPERIMENTAL MODEL AND SUBJECT DETAILS
 - Mice
- METHODS DETAILS
 - Generation and transfer of bone marrow-derived eosinophils
 - Infection, treatments, and bone marrow chimeras
 - Generation of over-expressing bone marrow chimeras
 - Transwell migration assay
 - 5-HIAA ELISA
 - Flow cytometry
 - Multiphoton *ex vivo* imaging, image analysis and PAS staining
- QUANTIFICATION AND STATISTICAL ANALYSIS

ACKNOWLEDGMENTS

We thank Serena Ranucci and Antonia Gallman for technical help and discussions. We thank Waliul Khan and Huaqing Wang for Tph1-deficient BM, Rebecca Krier and Paul Bryce for Cpa3-Cre mice, and Hong Liu and Gerard Karsenty for Tph1 floxed mice. M.D.G. was supported by an EMBO long-term fellowship and is supported by a CRI Irvington Postdoctoral Fellowship. J.G.C. is an investigator of the Howard Hughes Medical Institute. This work was supported by NIH grants R21AI163036, R01AI40098, and R01AI45073 to J.G.C. and R01AI165541 to H.D.M.

AUTHOR CONTRIBUTIONS

M.D.G. and J.G.C. conceptualized the study, designed the experiments, analyzed the data, and wrote the manuscript. E.V.D. and H.D.M. provided *C. neoformans*, expertise in the fungal infection model, helped design several experiments, and provided input on the manuscript. M.D.G. performed most experiments. E.V.D. performed initial *C. neoformans* infections and trained

M.D.G. in the fungal infection model. K.Y.C. performed some of the *in vitro* assay repeats. J.A. performed mouse screening.

DECLARATION OF INTERESTS

The authors declare no competing interests.

INCLUSION AND DIVERSITY

We support inclusive, diverse, and equitable conduct of research. One or more of the authors of this paper self-identifies as a member of the LGBTQ+ community.

Received: August 18, 2022

Revised: February 3, 2023

Accepted: May 10, 2023

Published: June 5, 2023

REFERENCES

1. Brown, G.D., Denning, D.W., Gow, N.A., Levitz, S.M., Netea, M.G., and White, T.C. (2012). Hidden killers: human fungal infections. *Sci. Transl. Med.* *4*, 165rv113. <https://doi.org/10.1126/scitranslmed.3004404>.
2. Saluja, R., Metz, M., and Maurer, M. (2012). Role and relevance of mast cells in fungal infections. *Front. Immunol.* *3*, 146. <https://doi.org/10.3389/fimmu.2012.00146>.
3. Mok, A.C., Mody, C.H., and Li, S.S. (2021). Immune cell degranulation in fungal Host Defence. *J. Fungi (Basel)* *7*. <https://doi.org/10.3390/jof7060484>.
4. Iyer, K.R., Revie, N.M., Fu, C., Robbins, N., and Cowen, L.E. (2021). Treatment strategies for cryptococcal infection: challenges, advances and future outlook. *Nat. Rev. Microbiol.* *19*, 454–466. <https://doi.org/10.1038/s41579-021-00511-0>.
5. Lopes, J.P., Stylianou, M., Backman, E., Holmberg, S., Ekoff, M., Nilsson, G., and Urban, C.F. (2019). *Cryptococcus neoformans* Induces MCP-1 release and delays the death of human mast cells. *Front. Cell. Infect. Microbiol.* *9*, 289. <https://doi.org/10.3389/fcimb.2019.00289>.
6. Decken, K., Köhler, G., Palmer-Lehmann, K., Wunderlin, A., Mattner, F., Magram, J., Gately, M.K., and Alber, G. (1998). Interleukin-12 is essential for a protective Th1 response in mice infected with *Cryptococcus neoformans*. *Infect. Immun.* *66*, 4994–5000. <https://doi.org/10.1128/IAI.66.10.4994-5000.1998>.
7. Hoag, K.A., Lipscomb, M.F., Izzo, A.A., and Street, N.E. (1997). IL-12 and IFN-gamma are required for initiating the protective Th1 response to pulmonary cryptococcosis in resistant C.B-17 mice. *Am. J. Respir. Cell Mol. Biol.* *17*, 733–739. <https://doi.org/10.1165/ajrcmb.17.6.2879>.
8. Voelz, K., Lammas, D.A., and May, R.C. (2009). Cytokine signaling regulates the outcome of intracellular macrophage parasitism by *Cryptococcus neoformans*. *Infect. Immun.* *77*, 3450–3457. <https://doi.org/10.1128/IAI.00297-09>.
9. Leopold Wager, C.M., Hole, C.R., Wozniak, K.L., Olszewski, M.A., and Wormley, F.L., Jr. (2014). STAT1 signaling is essential for protection against *Cryptococcus neoformans* infection in mice. *J. Immunol.* *193*, 4060–4071. <https://doi.org/10.4049/jimmunol.1400318>.
10. Blackstock, R., and Murphy, J.W. (2004). Role of interleukin-4 in resistance to *Cryptococcus neoformans* infection. *Am. J. Respir. Cell Mol. Biol.* *30*, 109–117. <https://doi.org/10.1165/rcmb.2003-0156OC>.
11. Huffnagle, G.B., Boyd, M.B., Street, N.E., and Lipscomb, M.F. (1998). IL-5 is required for eosinophil recruitment, crystal deposition, and mononuclear cell recruitment during a pulmonary *Cryptococcus neoformans* infection in genetically susceptible mice (C57BL/6). *J. Immunol.* *160*, 2393–2400.
12. Müller, U., Stenzel, W., Köhler, G., Werner, C., Polte, T., Hansen, G., Schütze, N., Straubinger, R.K., Blessing, M., McKenzie, A.N., et al. (2007). IL-13 induces disease-promoting type 2 cytokines, alternatively activated macrophages and allergic inflammation during pulmonary infection of mice with *Cryptococcus neoformans*. *J. Immunol.* *179*, 5367–5377. <https://doi.org/10.4049/jimmunol.179.8.5367>.
13. Osterholzer, J.J., Surana, R., Milam, J.E., Montano, G.T., Chen, G.H., Sonstein, J., Curtis, J.L., Huffnagle, G.B., Toews, G.B., and Olszewski, M.A. (2009). Cryptococcal urease promotes the accumulation of immature dendritic cells and a non-protective T2 immune response within the lung. *Am. J. Pathol.* *174*, 932–943. <https://doi.org/10.2353/ajpath.2009.080673>.
14. Piehler, D., Stenzel, W., Grahner, A., Held, J., Richter, L., Köhler, G., Richter, T., Eschke, M., Alber, G., and Müller, U. (2011). Eosinophils contribute to IL-4 production and shape the T-helper cytokine profile and inflammatory response in pulmonary cryptococcosis. *Am. J. Pathol.* *179*, 733–744. <https://doi.org/10.1016/j.ajpath.2011.04.025>.
15. Hernandez, Y., Arora, S., Erb-Downward, J.R., McDonald, R.A., Toews, G.B., and Huffnagle, G.B. (2005). Distinct roles for IL-4 and IL-10 in regulating T2 immunity during allergic bronchopulmonary mycosis. *J. Immunol.* *174*, 1027–1036. <https://doi.org/10.4049/jimmunol.174.2.1027>.
16. Szymczak, W.A., Sellers, R.S., and Pirofski, L.A. (2012). IL-23 dampens the allergic response to *Cryptococcus neoformans* through IL-17-independent and -dependent mechanisms. *Am. J. Pathol.* *180*, 1547–1559. <https://doi.org/10.1016/j.ajpath.2011.12.038>.
17. Verma, A.H., Bueter, C.L., Rothenberg, M.E., and Deepe, G.S. (2017). Eosinophils subvert host resistance to an intracellular pathogen by instigating non-protective IL-4 in CCR2^{-/-} mice. *Mucosal Immunol.* *10*, 194–204. <https://doi.org/10.1038/mi.2016.26>.
18. Muniz, V.S., Weller, P.F., and Neves, J.S. (2012). Eosinophil crystalloid granules: structure, function, and beyond. *J. Leukoc. Biol.* *92*, 281–288. <https://doi.org/10.1189/jlb.0212067>.
19. Hogan, S.P., Rosenberg, H.F., Moqbel, R., Phipps, S., Foster, P.S., Lacy, P., Kay, A.B., and Rothenberg, M.E. (2008). Eosinophils: biological properties and role in health and disease. *Clin. Exp. Allergy* *38*, 709–750. <https://doi.org/10.1111/j.1365-2222.2008.02958.x>.
20. Barrett, N.A., and Austen, K.F. (2009). Innate cells and T helper 2 cell immunity in airway inflammation. *Immunity* *31*, 425–437. <https://doi.org/10.1016/j.immuni.2009.08.014>.
21. Chen, H., Xu, X., Teng, J., Cheng, S., Bunjhoo, H., Cao, Y., Liu, J., Xie, J., Wang, C., Xu, Y., et al. (2015). CXCR4 inhibitor attenuates allergen-induced lung inflammation by down-regulating MMP-9 and ERK1/2. *Int. J. Clin. Exp. Pathol.* *8*, 6700–6707.
22. Lukacs, N.W., Berlin, A., Schols, D., Skerij, R.T., and Bridger, G.J. (2002). AMD3100, a CXCR4 antagonist, attenuates allergic lung inflammation and airway hyperreactivity. *Am. J. Pathol.* *160*, 1353–1360. [https://doi.org/10.1016/S0002-9440\(10\)62562-X](https://doi.org/10.1016/S0002-9440(10)62562-X).
23. Pope, S.M., Fulkerson, P.C., Blanchard, C., Akei, H.S., Nikolaidis, N.M., Zimmermann, N., Molkentin, J.D., and Rothenberg, M.E. (2005). Identification of a cooperative mechanism involving interleukin-13 and eotaxin-2 in experimental allergic lung inflammation. *J. Biol. Chem.* *280*, 13952–13961. <https://doi.org/10.1074/jbc.M406037200>.
24. Li, H., Li, Y., Sun, T., Du, W., Zhang, Z., Li, D., and Ding, C. (2020). Integrative proteome and acetylome analyses of murine responses to *Cryptococcus neoformans* infection. *Front. Microbiol.* *11*, 575. <https://doi.org/10.3389/fmicb.2020.00575>.
25. Nail, S., Robert, R., Dromer, F., Marot-Leblond, A., and Senet, J.M. (2001). Susceptibilities of *Cryptococcus neoformans* strains to platelet binding *in vivo* and to the fungicidal activity of thrombin-induced platelet microbicidal proteins *in vitro*. *Infect. Immun.* *69*, 1221–1225. <https://doi.org/10.1128/IAI.69.2.1221-1225.2001>.
26. Pitchford, S.C., Momi, S., Giannini, S., Casali, L., Spina, D., Page, C.P., and Gresle, P. (2005). Platelet P-selectin is required for pulmonary eosinophil and lymphocyte recruitment in a murine model of allergic inflammation. *Blood* *105*, 2074–2081. <https://doi.org/10.1182/blood-2004-06-2282>.
27. Ramirez, G.A., Yacoub, M.R., Ripa, M., Mannina, D., Cariddi, A., Saporiti, N., Ciceri, F., Castagna, A., Colombo, G., and Dagna, L. (2018). Eosinophils from physiology to disease: A comprehensive review. *BioMed Res. Int.* *2018*, 9095275. <https://doi.org/10.1155/2018/9095275>.

28. Wiesner, D.L., Smith, K.D., Kashem, S.W., Bohjanen, P.R., and Nielsen, K. (2017). Different lymphocyte populations direct dichotomous eosinophil or neutrophil responses to pulmonary *Cryptococcus* infection. *J. Immunol.* **198**, 1627–1637. <https://doi.org/10.4049/jimmunol.1600821>.
29. De Giovanni, M., Tam, H., Valet, C., Xu, Y., Looney, M.R., and Cyster, J.G. (2022). GPR35 promotes neutrophil recruitment in response to serotonin metabolite 5-HIAA. *Cell* **185**, 815.e19–830.e19. <https://doi.org/10.1016/j.cell.2022.01.010>.
30. Kaya, B., Donas, C., Wuggenig, P., Diaz, O.E., Morales, R.A., Melhem, H., Swiss IBD Cohort Investigators, Hernandez, P.P., Kaymak, T., Das, S., et al. (2020). Lysophosphatidic acid-mediated GPR35 signaling in CX3CR1(+) macrophages regulates intestinal homeostasis. *Cell Rep.* **32**, 107979. <https://doi.org/10.1016/j.celrep.2020.107979>.
31. Boleij, A., Fathi, P., Dalton, W., Park, B., Wu, X., Huso, D., Allen, J., Besharati, S., Anders, R.A., Housseau, F., et al. (2021). G-protein coupled receptor 35 (GPR35) regulates the colonic epithelial cell response to enterotoxigenic *Bacteroides fragilis*. *Commun. Biol.* **4**, 585. <https://doi.org/10.1038/s42003-021-02014-3>.
32. Lin, L.C., Quon, T., Engberg, S., Mackenzie, A.E., Tobin, A.B., and Milligan, G. (2021). G protein-coupled receptor GPR35 suppresses lipid accumulation in hepatocytes. *ACS Pharmacol. Transl. Sci.* **4**, 1835–1848. <https://doi.org/10.1021/acspsci.1c00224>.
33. Schneditz, G., Elias, J.E., Pagano, E., Zaeem Cader, M., Saveljeva, S., Long, K., Mukhopadhyay, S., Arasteh, M., Lawley, T.D., Dougan, G., et al. (2019). GPR35 promotes glycolysis, proliferation, and oncogenic signaling by engaging with the sodium potassium pump. *Sci. Signal.* **12**. <https://doi.org/10.1126/scisignal.aau9048>.
34. Wyant, G.A., Yu, W., Doulamis, I.P., Nomoto, R.S., Saeed, M.Y., Duignan, T., McCully, J.D., and Kaelin, W.G., Jr. (2022). Mitochondrial remodeling and ischemic protection by G protein-coupled receptor 35 agonists. *Science* **377**, 621–629. <https://doi.org/10.1126/science.abm1638>.
35. Wen, T., Besse, J.A., Mingler, M.K., Fulkerson, P.C., and Rothenberg, M.E. (2013). Eosinophil adoptive transfer system to directly evaluate pulmonary eosinophil trafficking in vivo. *Proc. Natl. Acad. Sci. USA* **110**, 6067–6072. <https://doi.org/10.1073/pnas.1220572110>.
36. Pereira, J.P., An, J., Xu, Y., Huang, Y., and Cyster, J.G. (2009). Cannabinoid receptor 2 mediates the retention of immature B cells in bone marrow sinusoids. *Nat. Immunol.* **10**, 403–411.
37. Hirasawa, R., Shimizu, R., Takahashi, S., Osawa, M., Takayanagi, S., Kato, Y., Onodera, M., Minegishi, N., Yamamoto, M., Fukao, K., et al. (2002). Essential and instructive roles of GATA factors in eosinophil development. *J. Exp. Med.* **195**, 1379–1386. <https://doi.org/10.1084/jem.20020170>.
38. Yu, C., Cantor, A.B., Yang, H., Browne, C., Wells, R.A., Fujiwara, Y., and Orkin, S.H. (2002). Targeted deletion of a high-affinity GATA-binding site in the GATA-1 promoter leads to selective loss of the eosinophil lineage in vivo. *J. Exp. Med.* **195**, 1387–1395. <https://doi.org/10.1084/jem.20020656>.
39. Duerschmied, D., Suidan, G.L., Demers, M., Herr, N., Carbo, C., Brill, A., Cifuni, S.M., Mauler, M., Cicko, S., Bader, M., et al. (2013). Platelet serotonin promotes the recruitment of neutrophils to sites of acute inflammation in mice. *Blood* **121**, 1008–1015. <https://doi.org/10.1182/blood-2012-06-437392>.
40. Shah, S.A., Page, C.P., and Pitchford, S.C. (2017). Platelet-eosinophil interactions as a potential therapeutic target in allergic inflammation and asthma. *Front. Med. (Lausanne)* **4**, 129. <https://doi.org/10.3389/fmed.2017.00129>.
41. Yue, M., Hu, M., Fu, F., Ruan, H., and Wu, C. (2022). Emerging roles of platelets in allergic asthma. *Front. Immunol.* **13**, 846055. <https://doi.org/10.3389/fimmu.2022.846055>.
42. Page, C., and Pitchford, S. (2013). Neutrophil and platelet complexes and their relevance to neutrophil recruitment and activation. *Int. Immunopharmacol.* **17**, 1176–1184. <https://doi.org/10.1016/j.intimp.2013.06.004>.
43. Berger, M., Gray, J.A., and Roth, B.L. (2009). The expanded biology of serotonin. *Annu. Rev. Med.* **60**, 355–366. <https://doi.org/10.1146/annurev.med.60.042307.110802>.
44. Freitag, A., Wessler, I., and Racke, K. (1995). Characterization of 5-hydroxytryptamine release from isolated rabbit and rat trachea: the role of neuroendocrine epithelia cells and mast cells. *Naunyn Schmiedebergs Arch. Pharmacol.* **353**, 55–63. <https://doi.org/10.1007/BF00168916>.
45. Gershon, R.K., Askenase, P.W., and Gershon, M.D. (1975). Requirement for vasoactive amines for production of delayed-type hypersensitivity skin reactions. *J. Exp. Med.* **142**, 732–747. <https://doi.org/10.1084/jem.142.3.732>.
46. Lehtosalo, J.I., Uusitalo, H., Laakso, J., Palkama, A., and Härkönen, M. (1984). Biochemical and immunohistochemical determination of 5-hydroxytryptamine located in mast cells in the trigeminal ganglion of the rat and guinea pig. *Histochemistry* **80**, 219–223. <https://doi.org/10.1007/BF00495769>.
47. Sjoerdsma, A., Waalkes, T.P., and Weissbach, H. (1957). Serotonin and histamine in mast cells. *Science* **125**, 1202–1203. <https://doi.org/10.1126/science.125.3259.1202>.
48. Lilla, J.N., Chen, C.C., Mukai, K., BenBarak, M.J., Franco, C.B., Kalesnikoff, J., Yu, M., Tsai, M., Piliiponsky, A.M., and Galli, S.J. (2011). Reduced mast cell and basophil numbers and function in Cpa3-Cre; Mcl-1fl/fl mice. *Blood* **118**, 6930–6938. <https://doi.org/10.1182/blood-2011-03-343962>.
49. Dang, E.V., Lei, S., Radkov, A., Volk, R.F., Zaro, B.W., and Madhani, H.D. (2022). Secreted fungal virulence effector triggers allergic inflammation via TLR4. *Nature* **608**, 161–167. <https://doi.org/10.1038/s41586-022-05005-4>.
50. Bohrer, A.C., Castro, E., Tocheny, C.E., Assmann, M., Schwarz, B., Bohrsen, E., Makiya, M.A., Legrand, F., Hilligan, K.L., Baker, P.J., et al. (2022). Rapid GPR183-mediated recruitment of eosinophils to the lung after *Mycobacterium tuberculosis* infection. *Cell Rep.* **40**, 111144. <https://doi.org/10.1016/j.celrep.2022.111144>.
51. Deppermann, C., and Kubes, P. (2018). Start a fire, kill the bug: the role of platelets in inflammation and infection. *Innate Immun.* **24**, 335–348. <https://doi.org/10.1177/1753425918789255>.
52. Rapkiewicz, A.V., Mai, X., Carsons, S.E., Pittaluga, S., Kleiner, D.E., Berger, J.S., Thomas, S., Adler, N.M., Charytan, D.M., Gasmi, B., et al. (2020). Megakaryocytes and platelet-fibrin thrombi characterize multi-organ thrombosis at autopsy in COVID-19: A case series. *EClinicalmedicine* **24**, 100434. <https://doi.org/10.1016/j.eclinm.2020.100434>.
53. Cheng, L.E., Hartmann, K., Roers, A., Krummel, M.F., and Locksley, R.M. (2013). Perivascular mast cells dynamically probe cutaneous blood vessels to capture immunoglobulin E. *Immunity* **38**, 166–175. <https://doi.org/10.1016/j.immuni.2012.09.022>.
54. Dudeck, J., Kotrba, J., Immler, R., Hoffmann, A., Voss, M., Alexaki, V.I., Morton, L., Jahn, S.R., Katsoulis-Dimitriou, K., Winzer, S., et al. (2021). Directional mast cell degranulation of tumor necrosis factor into blood vessels primes neutrophil extravasation. *Immunity* **54**, 468.e5–483.e5. <https://doi.org/10.1016/j.immuni.2020.12.017>.
55. Garcia-Rodriguez, K.M., Bini, E.I., Gamboa-Dominguez, A., Espitia-Pinzón, C.I., Huerta-Yepez, S., Bulfone-Paus, S., and Hernández-Pando, R. (2021). Differential mast cell numbers and characteristics in human tuberculosis pulmonary lesions. *Sci. Rep.* **11**, 10687. <https://doi.org/10.1038/s41598-021-89659-6>.
56. Karhausen, J., Choi, H.W., Maddipati, K.R., Mathew, J.P., Ma, Q., Boulaftali, Y., Lee, R.H., Bergmeier, W., and Abraham, S.N. (2020). Platelets trigger perivascular mast cell degranulation to cause inflammatory responses and tissue injury. *Sci. Adv.* **6**, eaay6314. <https://doi.org/10.1126/sciadv.aay6314>.
57. Kunder, C.A., St John, A.L., and Abraham, S.N. (2011). Mast cell modulation of the vascular and lymphatic endothelium. *Blood* **118**, 5383–5393. <https://doi.org/10.1182/blood-2011-07-358432>.

58. Hargarten, J. (2021). Characterization of a GPR35 nonsense mutation in a previously healthy patient with non-HIV cryptococcal meningoencephalitis. NIH FARE2021 abstract. https://www.training.nih.gov/assets/FARE2021_Winners_Sorted_by_Institute_Center.pdf.
59. Rhein, J., Morawski, B.M., Hullsiek, K.H., Nabeta, H.W., Kiggundu, R., Tugume, L., Musubire, A., Akampurira, A., Smith, K.D., Alhadab, A., et al. (2016). Efficacy of adjunctive sertraline for the treatment of HIV-associated cryptococcal meningitis: an open-label dose-ranging study. *Lancet Infect. Dis.* 16, 809–818. [https://doi.org/10.1016/S1473-3099\(16\)00074-8](https://doi.org/10.1016/S1473-3099(16)00074-8).
60. Loulergue, P., Mir, O., Rocheteau, P., Chrétien, F., and Gaillard, R. (2016). Sertraline-induced increase in VEGF brain levels and its activity in cryptococcal meningitis. *Lancet Infect. Dis.* 16, 891. [https://doi.org/10.1016/S1473-3099\(16\)30147-5](https://doi.org/10.1016/S1473-3099(16)30147-5).
61. Zhai, B., Wu, C., Wang, L., Sachs, M.S., and Lin, X. (2012). The antidepressant sertraline provides a promising therapeutic option for neurotropic cryptococcal infections. *Antimicrob. Agents Chemother.* 56, 3758–3766. <https://doi.org/10.1128/AAC.00212-12>.
62. Lefrançois, E., Ortiz-Muñoz, G., Caudrillier, A., Mallavia, B., Liu, F., Sayah, D.M., Thornton, E.E., Headley, M.B., David, T., Coughlin, S.R., et al. (2017). The lung is a site of platelet biogenesis and a reservoir for haematopoietic progenitors. *Nature* 544, 105–109. <https://doi.org/10.1038/nature21706>.
63. Yadav, V.K., Ryu, J.H., Suda, N., Tanaka, K.F., Gingrich, J.A., Schütz, G., Glorieux, F.H., Chiang, C.Y., Zajac, J.D., Insogna, K.L., et al. (2008). Lrp5 controls bone formation by inhibiting serotonin synthesis in the duodenum. *Cell* 135, 825–837. <https://doi.org/10.1016/j.cell.2008.09.059>.
64. Bengel, D., Murphy, D.L., Andrews, A.M., Wichems, C.H., Feltner, D., Heils, A., Mössner, R., Westphal, H., and Lesch, K.P. (1998). Altered brain serotonin homeostasis and locomotor insensitivity to 3, 4-methylenedioxymethamphetamine ("Ecstasy") in serotonin transporter-deficient mice. *Mol. Pharmacol.* 53, 649–655. <https://doi.org/10.1124/mol.53.4.649>.
65. Lefrançois, E., Mallavia, B., Zhuo, H., Calfee, C.S., and Looney, M.R. (2018). Maladaptive role of neutrophil extracellular traps in pathogen-induced lung injury. *JCI Insight* 3. <https://doi.org/10.1172/jci.insight.98178>.
66. Côté, F., Thévenot, E., Fligny, C., Fromes, Y., Darmon, M., Ripoché, M.A., Bayard, E., Hanoun, N., Saurini, F., Lechat, P., et al. (2003). Disruption of the nonneuronal tph1 gene demonstrates the importance of peripheral serotonin in cardiac function. *Proc. Natl. Acad. Sci. USA* 100, 13525–13530. <https://doi.org/10.1073/pnas.2233056100>.
67. Liu, D., Duan, L., Rodda, L.B., Lu, E., Xu, Y., An, J., Qiu, L., Liu, F., Looney, M.R., Yang, Z., et al. (2022). CD97 promotes spleen dendritic cell positioning and homeostasis through the mechanosensing of red blood cells. *Science* 375, eabi5965. <https://doi.org/10.1126/science.abi5965>.
68. Muzumdar, M.D., Tasic, B., Miyamichi, K., Li, L., and Luo, L. (2007). A global double-fluorescent Cre reporter mouse. *Genesis* 45, 593–605. <https://doi.org/10.1002/dvg.20335>.

STAR★METHODS

KEY RESOURCES TABLE

REAGENT or RESOURCE	SOURCE	IDENTIFIER
Antibodies		
PerCP/Cy5.5 rat anti-mouse CD45.1 (A20)	BioLegend	Cat# 110728; RRID: AB_893346
FITC-conjugated rat anti-mouse CD45.2 (104)	BioLegend	Cat# 109806; RRID: AB_313443
BV785-conjugated rat anti-mouse SiglecF (E50-2440)	BD	Cat# 740956; RRID: AB_2740581
PE-conjugated rat anti-mouse SiglecF (E50-2440)	BioLegend	Cat# 552126; RRID: AB_394341
BV785-conjugated rat anti-mouse/human CD11b (M1/70)	BioLegend	Cat# 101243; RRID: AB_2561373
PE-conjugated rat anti-mouse/human CD11b (M1/70)	BioLegend	Cat# 101208; RRID: AB_312791
APC-conjugated rat anti-mouse CD64 (X54-5/7.1)	BioLegend	Cat# 139306; RRID: AB_11219391
BV605-conjugated rat anti-mouse CD45.2 (104)	BioLegend	Cat# 109841; RRID: AB_2563485
PB-conjugated rat anti-mouse CD45.2 (104)	BioLegend	Cat# 109820; RRID: AB_492872
BV605-conjugated rat anti-mouse CD45.1 (A20)	BioLegend	Cat# 110738; RRID: AB_378458
AF700-conjugated rat anti-mouse CD45.1 (A20)	BioLegend	Cat# 110724; RRID: AB_493733
PB-conjugated rat anti-mouse CD45.1 (A20)	BioLegend	Cat# 110722; RRID: AB_492866
APC-Cy7-conjugated rat anti-mouse Ly6G (1A8)	TONBO	Cat# 25-1276; RRID: AB_2621632
FITC-conjugated rat anti-mouse Ly6C (AL-21)	BD	Cat# 553104; RRID: AB_394628
BV605-conjugated rat anti-mouse Ly6C (HK1.4)	BioLegend	Cat# 128036; RRID: AB_2562353
BV650-conjugated rat anti-mouse Ly6C (HK1.4)	BioLegend	Cat# 128049; RRID: AB_2800630
BV570-conjugated rat anti-mouse/human CD11b (M1/70)	BioLegend	Cat# 101233; RRID: AB_10896949
FITC-conjugated rat anti-mouse CD41 (MWRReg30)	BioLegend	Cat# 133903; RRID: AB_1626237
PE-conjugated anti-mouse CD45.2 (104)	BioLegend	Cat# 109808; RRID: AB_313445
PerCP/Cy5.5-conjugated rat anti-mouse CD4 (GK1.5)	BioLegend	Cat# 100434; RRID: AB_893324
FITC-conjugated rat anti-mouse CD44 (IM7)	BioLegend	Cat# 103006; RRID: AB_312957
BV421-conjugated rat anti-mouse TCR β chain (H57-597)	BioLegend	Cat# 109230; RRID: AB_2562562
APC-Cy7-conjugated rat anti-mouse CD62L (MEL-14)	BioLegend	Cat# 104428; RRID: AB_830799
PE-conjugated rat anti mouse/human GATA3 (REA174)	Miltenyi	Cat# 130-100-664; RRID: AB_2651823
Alexa647-conjugated rat anti mouse anti-T-bet (4B10)	BioLegend	Cat# 644803; RRID: AB_1595573
APC-conjugated anti-mouse IL-4 (11B11)	eBioscience	Cat# 17-7041-82; RRID: AB_469494
PE/Cy7-conjugated rat anti-mouse IFN γ (XMG1.2)	BioLegend	Cat# 505826; RRID: AB_2295770
APC anti-mouse IFN γ (XMG1.2)	BioLegend	Cat# 505810; RRID: AB_315404
Rabbit polyclonal anti-GPR35	Biomatik	N/A
AF647-Goat anti-Rabbit IgG (H+L) Highly Cross-Adsorbed Ab	Fisher Scientific	Cat# A21245; RRID: AB_2535813
Bacterial and virus strains		
<i>Cryptococcus neoformans</i> (strain KN99)	Madhani lab, UCSF	N/A
Chemicals, peptides, and recombinant proteins		
5-HIAA	Sigma	#H8876
CXCL12 (SDF1a human)	Peptide	#300-28A
Diphtheria Toxin (DT)	Millipore/Sigma	#322326
FMS-like tyrosine kinase 3 ligand (Peptide)	Peptide	#250-31
IL-5	Peptide	#215-15
IL-3	Peptide	#213-13
IL-6	Peptide	#216-16
Stem Cell Factor	Peptide	#250-03
Cell Trace Violet	Fisher	#C34557
Deep Red	Life Tech	#C34565

(Continued on next page)

REAGENT or RESOURCE	SOURCE	IDENTIFIER
Continued		
Critical commercial assays		
Mouse 5-Hydroxyindoleacetic acid (5HIAA 5-HIAA) ELISA Kit	AssayGenie	# MOEB2528
Experimental models: Cell lines		
Plat-e cells	Susan Schwab lab, NYU	N/A
Experimental models: Organisms/strains		
C57BL/6J	Jackson	B6 background
BoyJ (CD45.1)	Jackson	B6 background
Gpr35 ^{-/-}	EMMA (EM09677; Gpr35tm1b(EUCOMM)Hmgu)	B6 background
Pf4-Cre x mTmG (Gt(ROSA)26Sortm4 (ACTB-tdTomato,-EGFP)Luo/J)	Looney lab, UCSF ⁶²	B6 background
Kit ^v x Kit ^W	Jackson	B6 background
TPH1 het and ko (Bone Marrow)	Huaqing Wang and Waliul Khan lab, McMaster Univ.	B6 background
GATA1-deficient ΔdbiGATA (C.129S1(B6)-Gata1tm6Sho/J)	Jackson	B6 background
Tph1 floxed mice	Gerard Karsenty, Columbia Univ. ⁶³	B6 background
Cpa3-Cre mice	Paul Bryce, Northwestern Univ. ⁴⁸	B6 background
SERT-deficient mice (B6.129(Cg)-Slc6a4tm1Kpl/J)	Jackson ⁶⁴	B6 background
Oligonucleotides		
ACGCGGGGACAGAGGTATG-Fwd (Gpr35 qPCR)		N/A
TGAGGGTGCTTACAGGTTG-Rev (Gpr35 qPCR)		N/A
Software and algorithms		
IMARIS (v.9.6.0)		N/A
Flowjo (v.10.6.2)		N/A
Prism (GraphPad 9.0.1)		N/A
Seurat R package (version 2.2)		N/A
R studio (3.5)		N/A

RESOURCE AVAILABILITY

Lead contact

Further information and requests for reagents will be fulfilled by Dr. Jason Cyster (jason.cyster@ucsf.edu).

Materials availability

A list of critical reagents (key resources) is included in the [key resources table](#). Some material may require requests to collaborators and/or agreements with various entities. Material that can be shared will be released via a Material Transfer Agreement.

Data and code availability

All data reported in this paper are available in the main text or [supplemental information](#).

This paper does not report original code. Any additional information required to reanalyze the data reported in this work paper is available from the [lead contact](#) upon request.

EXPERIMENTAL MODEL AND SUBJECT DETAILS

Mice

C57BL/6J and BoyJ (CD45.1) mice were bred in an internal colony and 7–12-week-old mice of both sexes were used. *Gpr35*^{-/-} mice were obtained from EMMA (EM09677; *Gpr35*^{tm1b}(EUCOMM)Hmgu) and maintained on a B6 background. Platelet-deficient mice (*cmp1*^{-/-}), Pf4-Cre x mTmG (Gt(ROSA)26Sortm4(ACTB-tdTomato,-EGFP)Luo/J) platelet reporter mice^{62,65} and CD11c-DTR-GFP mice were all on a B6 background. Mast cell-deficient Kit/v x Kit/W mice and SERT-deficient mice⁶⁴ were obtained from Jackson Laboratories and maintained on a B6 background. *Tph1*^{+/-} and *Tph1*^{-/-66} BM were provided by Huaqing Wang and Waliul Khan (McMaster Univ.). GATA1-deficient Δ dblGATA1 (C.129S1(B6)-Gata1^{tm6Sho}/J) mice were obtained from Jackson Laboratories. Tph1 floxed mice⁶³ were kindly provided by Gerard Karsenty (Columbia Univ.). Cpa3-Cre mice⁴⁸ were kindly provided by Paul Bryce (Northwestern Univ). Co-caged littermate controls (+/+, +/- and -/-) were used for experiments, mice were allocated to control and experimental groups randomly, sample sizes were chosen based on previous experience to obtain reproducible results and the investigators were not blinded.

METHODS DETAILS

Generation and transfer of bone marrow-derived eosinophils

To produce BM-derived eosinophil, total BM cells were isolated from *GPR35*^{+/+} and *GPR35*^{-/-} and cultured in Iscove's modified Dulbecco's media (IMDM) (#12440053; Fisher), containing 10% heat-inactivated FBS (#FB-02; Omega Scientific), 1% Pen Strep (#MT-30-001-CI; Fisher), 2 mM glutamine (#MT 25-005-CI; Fisher), and 55 μ M 2-mercaptoethanol (#21985023; Fisher). During the 14-day culture, medium was supplemented with FMS-like tyrosine kinase 3 ligand (# 250-31, Peprotech) and stem cell factor (#250-03, Peprotech) at 100 ng/mL, for the first 4 days. At day 4, medium was removed and fresh IMDM supplemented with IL-5 (10 ng/mL, #215-15, Peprotech) was added for the following 10 days, similarly to what was previously described.³⁵ Eosinophil purity (>95%) was checked before cell transfer by flow cytometry (using SiglecF, CD64 and CD11b staining). For co-transfer experiments, BM-derived *GPR35*^{+/+} and *GPR35*^{-/-} eosinophils were labeled for 30 min at 37°C with Cell trace Violet (#C34557, Fisher) or Deep red (#C34565, Life Tech) similarly to what was previously described²⁹ and mixed 50:50 before injection (3 x 10⁷ eosinophil / mouse in 200 μ l saline) in mice previously infected with *C. neoformans* (day 5).

Infection, treatments, and bone marrow chimeras

Cryptococcus neoformans (strain KN99) was from the Madhani lab. Individual colonies from *C. neoformans* plates were cultured overnight in 10 ml YPAD at 30 °C. The next day, yeast were counted on a hemocytometer and diluted to 2 x 10⁶ cells/ml in saline. Mice were anaesthetized with a mixture of oxygen and Isoflurane and then hung by their front teeth using surgical thread. 50 μ l yeast (1 x 10⁵ CFU) were then pipetted onto the nasal flares and taken up by aspiration, as previously described.⁴⁹ To deplete total generation of 5-HIAA, mice were treated i.p. with Phenelzine (30mg/kg, #P6777, Millipore Sigma) starting 3 days before infection. The treatment was repeated every other day (15mg/kg) until the end of the experiment. To produce mixed chimeras, CD45.1 congenic Boy/J mice were lethally irradiated with 1300 rad in split doses and reconstituted with 5 x 10⁶ BM cells (~50:50) as indicated. Mice were analyzed 7-8 weeks later. Since the hematopoietic stem cell content in BM from different donor mice may not be identical, reconstitution of the B220⁺ B cell compartment was used to assess chimerism after reconstitution. B cells lack GPR35 expression and are not expected to be affected by GPR35-deficiency. Animals were housed in a pathogen-free environment in the Laboratory Animal Resource Center at the University of California, San Francisco, and all experiments conformed to ethical principles and guidelines that were approved by the Institutional Animal Care and Use Committee. To generate mice with full GPR35-deficiency restricted to dendritic cells, CD11c-DTR-GFP BM was mixed 1:1 with *GPR35*^{+/+} or *GPR35*^{-/-} BM and used to reconstitute WT mice. After 7 weeks reconstitution the chimeras were treated with 20ng/g diphtheria toxin i.v. (DT, #322326, Millipore) starting 3 days before infection and every other day with 80ng DT (i.v.). To generate mice with full GPR35-deficiency restricted to eosinophils, Δ dblGATA1 BM was mixed 1:1 with *GPR35*^{+/+} or *GPR35*^{-/-} BM and used to reconstitute WT mice. Chimeric mice were infected 7-8 weeks after reconstitution. For detection of cells within the vascular system versus parenchyma of the lung, mice were injected with 2 μ g of anti-CD45.2-PE 5 min before sacrifice and tissue isolation. During this short period of in vivo antibody exposure, cells in blood vessels and blood exposed spaces become labeled while cells in the parenchyma remain unlabeled.³⁶

Generation of over-expressing bone marrow chimeras

Mice to be used as BM donors (C57BL/6J) were injected intravenously with 3 mg 5-fluorouracil (Sigma). BM was collected after 4 days and cultured in DMEM containing 15% (v/v) FBS, antibiotics (penicillin (50 IU/ml) and streptomycin (50mg/ml); Fisher) and 10 mM HEPES, pH 7.2 (Cellgro), supplemented with IL-3 (#213-13, Peprotech), IL-6 (#216-16, Peprotech) and stem cell factor (#250-03, Peprotech) at concentrations of 20, 50 or 100 ng/ml, respectively). Cells were spininfected twice at days 1 and 2 with viral supernatant (MSCV-EV-GFP and MSCV-GPR35-GFP) and transferred into irradiated CD45.1 B6 recipient mice on day 3, similarly to what was previously described.⁶⁷

Transwell migration assay

GPR35^{+/+}(CD45.1⁺) and *GPR35*^{-/-} (CD45.2⁺) lungs were mashed in 70 μ m strainers and resuspended in 5ml of migration medium (RPMI containing 0.5% fatty acid-free BSA, 10 mM HEPES and 50 IU/L penicillin/streptomycin RPMI) in 15ml conical tubes. Samples

were centrifuged at 20g (300 rpm) for 3 minutes to remove large clumps and cell-containing supernatants were transferred into clean 15ml conical tubes. Samples were then centrifuged at 526g (1500 rpm) for 5 minutes and pellets were ACK lysed. Cells were washed twice in pre-warmed migration medium and mixed 50:50 (CD45.1:CD45.2). The cells were resuspended in migration medium at 2.5×10^6 cells/ml and resensitized for 30 min in a 37 °C water bath in migration plus medium. Transwell filters (6 mm insert, 5 μm pore size, Corning) were placed on top of each well, and 100 μl containing 2.5×10^5 cells was added to the transwell insert. In some cases cells were pretreated with pertussis toxin (100ng/ml) for 2 hr prior to the assay. 600ul of chemoattractant (5-HIAA at indicated concentrations, CXCL12 100ng/ml or CCL11 1ug/ml) or no chemoattractant (Nil) was added to the lower well. The cells were allowed to migrate for 3 hr, after which the cells in the bottom well were counted by flow cytometry. Representative experiments for each migration assay are plotted as a percentage of input migration.

5-HIAA ELISA

5-HIAA (#H8876) was purchased from Sigma and diluted in DMSO. To quantify 5-HIAA concentrations, lungs were weighed, carefully minced into small pieces and mashed through 100μm strainer (Fisher Scientific) in 1ml PBS per g of tissue (1ml/g). Samples were then centrifuged at 10000 rpm for 30min at 4°C to obtain lung supernatants. To quantify 5-HIAA, Mouse 5-Hydroxyindoleacetic acid (5-HIAA) ELISA Kit (AssayGenie) was used following manufacturer instructions.

Flow cytometry

Eosinophils were identified as CD45⁺ SiglecF⁺ CD64⁻ CD11b⁺ or CD45⁺ SiglecF⁺ CD64⁻ cells as indicated. Cells were stained with the following antibodies: PerCP/Cy5.5 rat anti-mouse CD45.1 (A20, #110728); FITC-conjugated rat anti-mouse CD45.2 (104, #109806, BioLegend); BV785-conjugated rat anti-mouse SiglecF (E50-2440, #740956; BD); PE-conjugated rat anti-mouse SiglecF (E50-2440, #552126, BioLegend); BV785-conjugated rat anti-mouse/human CD11b (M1/70, #101243, BioLegend); PE-conjugated rat anti-mouse/human CD11b (M1/70, #101208, BioLegend); APC-conjugated rat anti-mouse CD64 (X54-5/7.1, #139306, BioLegend). For mixed chimeras experiments the following additional antibodies were used to discriminate between GPR35^{+/+} and GPR35^{-/-} cells: BV605-conjugated rat anti-mouse CD45.2 (104, #109841, BioLegend); PB-conjugated rat anti-mouse CD45.2 (104, #09820, BioLegend); BV605-conjugated rat anti-mouse CD45.1 (A20, #110738, BioLegend); AF700-conjugated rat anti-mouse CD45.1 (A20, #110724, BioLegend); PB-conjugated rat anti-mouse CD45.1 (A20, #110722, BioLegend). To identify neutrophils, monocytes and alveolar macrophages, the following antibodies (in addition to previous ones) were used: APC-Cy7-conjugated rat anti-mouse Ly6G (1A8, #25-1276, TONBO); FITC-conjugated rat anti-mouse Ly6C (AL-21, #553104, BD); BV605-conjugated rat anti-mouse Ly6C (HK1.4, #128036, BioLegend); BV650-conjugated rat anti-mouse Ly6C (HK1.4, #128049, BioLegend); BV570-conjugated rat anti-mouse/human CD11b (M1/70, #101233, BioLegend). For flow cytometry on lung samples, mice were infected or challenged as indicated and then lungs were dissected and minced using scissors. The minced lung tissue was then incubated for 30 min shaking (1000rpm) at 37 °C in 1ml of digestion medium (RPMI, 1% NBCS, 0.25 mg ml⁻¹, Liberase TM Research Grade (Sigma), 0.025 mg ml⁻¹ DNaseI (Sigma)). To stop the digestion, 100μl of quenching solution (RPMI, 0.1M EDTA, 50% NBCS) were added to each sample. The digested lung tissue was then mashed through a 100-μm strainer (Fisher Scientific) and washed with in RPMI (2% FCS, 1 mM EDTA). Spleens were mashed through a 100-μm strainer 70-μm in RPMI, 1%NBCS, 0.1m EDTA. Blood was collected by retro-orbital bleeding using heparinized micro-hematocrit capillary tubes (Fisher). Red blood cells were then lysed (2x) for 5 min on ice using ACK Lysis Buffer. Cells were resuspended in FACS buffer (1 × PBS, 2% FCS, 1 mM EDTA) for staining. To identify intravascular cells, 2 μg/200μl saline of PE-conjugated anti-mouse CD45.2 (104, #109806, BioLegend) were injected 5 min before sacrifice as indicated. To identify Th1 and Th2 cells in infected lungs, lung cell surface markers were stained with the following antibodies: BV605-conjugated rat anti-mouse CD45.2 (104, #109841, BioLegend); PerCP/Cy5.5-conjugated rat anti-mouse CD4 (GK1.5, #100434, BioLegend); FITC-conjugated rat anti-mouse CD44 (IM7, #103006, BioLegend); BV421-conjugated rat anti-mouse TCR β chain (H57-597, #109230, BioLegend); APC-Cy7-conjugated rat anti-mouse CD62L (MEL-14, #104428, BioLegend). Cells were then washed, fixed/permeabilized (FoxP3 fixation/permeabilization concentrate and diluent, eBioscience) and stained with the following antibodies: PE-conjugated rat anti mouse/human GATA3 (REA174, #130-100-664, Miltenyi); Alexa647-conjugated rat anti mouse anti-T-bet (4B10, #644803, BioLegend). For ex vivo re-stimulation, processed lung cells from *Cryptococcus* infected GPR35^{+/+} and GPR35^{-/-} full BM chimeras (day 11) were incubated with resting medium (RPMI containing 10% FBS, 10 mM HEPES, 2 mM glutamine and 50 IU/L penicillin/streptomycin plus GolgiPlug Protein Transport Inhibitor (#555029, BD)) or stimulation medium (RPMI containing 10% FBS, 10 mM HEPES, 2 mM glutamine and 50 IU/L penicillin/streptomycin plus GolgiPlug Protein Transport Inhibitor and PMA/Ionomycin (Millipore Sigma) for 3.5 hours at 37°C. Cells were then washed and stained for the surface markers with the following antibodies: BV605-conjugated rat anti-mouse CD45.2 (104, #109841, BioLegend); PerCP/Cy5.5-conjugated rat anti-mouse CD4 (GK1.5, #100434, BioLegend); FITC-conjugated rat anti-mouse CD44 (IM7, #103006, BioLegend); BV421-conjugated rat anti-mouse TCR β chain (H57-597, #109230, BioLegend); APC-Cy7-conjugated rat anti-mouse CD62L (MEL-14, #104428, BioLegend). Cells were then washed, fixed/permeabilized (Cytofix/Cytoperm Fixation and Permeabilization Solution, BD) and stained with the following antibodies APC-conjugated anti-mouse IL-4 (11B11, #17-7041-82, eBioscience); PE/Cy7-conjugated rat anti-mouse IFNγ (XMG1.2, #505826); APC anti-mouse IFNγ (XMG1.2, #505810). Rabbit polyclonal anti-GPR35 was produced by Biomatik (using as immunogen the C terminus peptide: MAREFQEASKPATSSNTPHKSQDSQILSLT) and affinity-purified. To reduce non-specific background, anti-GPR35 polyclonal antibody was pre-absorbed against GPR35^{-/-} lung cells overnight at 4°C. Cells were surface-stained, fixed and permeabilized (eBioscience™, #00552100) before intracellular staining. AF647-Goat anti-Rabbit IgG (H+L) Highly Cross-Adsorbed Ab (A21245, Fisher Scientific) was used as secondary antibody. To quantify

eosinophil-platelet interaction, 100 μ l of blood were obtained by retro-orbital bleeding (heparinized capillaries) and drawn into tubes containing 1 ml of Lyse/Fix Buffer 5X (Ox-7, #558049, BioLegend) and incubated for 15 min. Cells were then washed and resuspended in staining buffer. FITC-conjugated anti-mouse CD41 (MWRReg30, # 133903, BioLegend) was used to stain eosinophils that acquired platelet membrane material. Data were acquired using a BD LSR II flow cytometer or a Cytex Aurora. Flow cytometry data were analyzed using Flowjo (v.10.6.2).

Multiphoton *ex vivo* imaging, image analysis and PAS staining

To perform multiphoton *ex vivo* imaging of eosinophil and platelet interactions, we injected 1.5×10^7 (50:50, in 200 μ l saline) of Cell Trace Violet-labeled (CTV, # C34557, Life Tech) GPR35^{+/+} and Deep Red-labeled (#C34565, Life Tech) GPR35^{-/-} BM-derived eosinophils in Pf4-Cre x mTmG previously i.n. infected with *C. neoformans* (day 5). Pf4Cre mTmG mice expressed GFP selectively in platelets; these mice broadly expressed tdTom in other cell types including neutrophils but the intensity of red fluorescence in these cells was weak as reported.⁶⁸ Accordingly, platelet and vessels were identified based on GFP signal and tdTomato signal, respectively. To further define the vessel lumen, tetramethylrhodamine isothiocyanate (TRITC) Dextran (150kDa, # T1287, Sigma) was injected 20 min before mouse euthanasia. Mice were euthanized 6 hrs after cell transfer and infected lungs were dissected, washed with PBS and cut into pieces (~ 0.1 - 0.3 cm³) that were glued (VetBond) on Superfrost Plus Microscope Slides (Fisher). Samples were immersed in PBS and imaged with a Zeiss LSM 7MP equipped with a Chameleon laser (Coherent) and a x20 objective. Samples were excited at 820-850nm. For image acquisition, a series of planes of 3 μ m z-spacing spanning a depth of 30-60 μ m were collected. Multiphoton images were imported into IMARIS software (v.9.6.0). Vessel surface was obtained using IMARIS built-in surface function based on dextran-TRITC plus TdTomato (mTmG) signal as indicated. IMARIS built-in functions 'Background subtraction' and 'Gaussian Filter' were applied. To track single cells and platelets, surface seed points were created and tracked with IMARIS spot built-in function based on signal intensity.

To perform PAS staining, *Cryptococcus* infected lungs were cut into 3mm pieces and fixed overnight in 4% PFA at 4°C. After 12-18 hrs, the samples were washed and incubated in 70% ethanol for 72 hrs at 4°C. Lung slices (4 μ m) were prepared and stained by the BTBTC Core (UCSF).

QUANTIFICATION AND STATISTICAL ANALYSIS

Prism software (GraphPad 9.0.1) was used for all statistical analyses. The statistical tests used are specified in the figure legends. Two-tailed unpaired t-tests were performed when comparing only two groups, Paired- t-tests were used to compare internally controlled replicates, and ordinary one-way ANOVA using Turkey's multiple comparisons test was performed when comparing one variable across multiple groups. $P < 0.05$ was considered significant. In summary graphs, points indicate individual samples and horizontal lines are means or medians as indicated. In bar graphs, bars show means and error bars indicate standard error mean (SEM).

Immunity, Volume 56

Supplemental information

**Platelets and mast cells promote pathogenic
eosinophil recruitment during invasive fungal
infection via the 5-HIAA-GPR35 ligand-receptor system**

**Marco De Giovanni, Eric V. Dang, Kevin Y. Chen, Jinping An, Hiten D. Madhani, and Jason
G. Cyster**

Figure S1

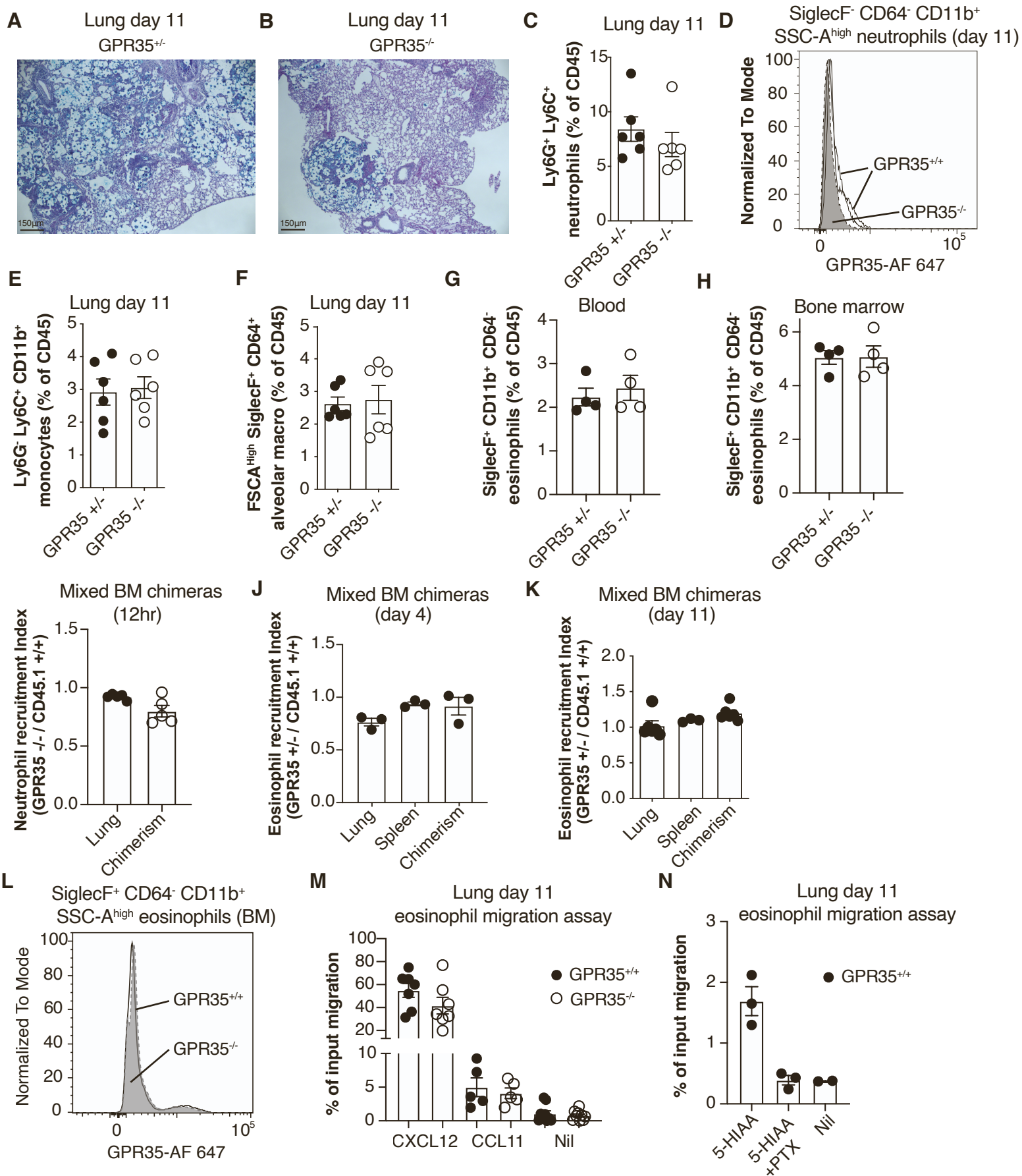


Figure S1, Related to Figures 1 and 2. GPR35 function in myeloid cell recruitment to the lung shows selectivity for eosinophils. (A, B) Representative lung sections from infected GPR35^{+/-} (A) and GPR35^{-/-} (B) indicate better fungal control in the absence of GPR35 at day 11 after infection. PAS staining was performed. Images are representative of 4 mice of each type. (C) Quantification of Ly6G⁺ Ly6C⁺ neutrophil percentages out of CD45⁺ cells in *C. neoformans* infected lungs from GPR35^{+/+} and GPR35^{-/-} mice. n=6. Data are pooled from 2 independent experiments. (D) Flow cytometry histograms showing levels of GPR35 in SSC-A-high SiglecF⁻ CD64⁻ CD11b⁺ neutrophils in lung from GPR35^{+/+} (white) and GPR35^{-/-} (black) mice, 11 days after infection. Data are representative of 2 independent experiments. (E, F) Quantification of Ly6G⁻ Ly6C⁺ CD11b⁺ monocyte (E) and FSC-A-high SiglecF⁺ CD64⁺ CD11b⁺ alveolar macrophage (F) percentages in lungs of *C. neoformans* infected GPR35^{+/+} and GPR35^{-/-} full chimeras, 11 days after intranasal infection. n=6. Data are pooled from 2 independent experiments. (G, H) Quantification of SiglecF⁺ CD11b⁺ CD64⁻ eosinophil percentages in blood (G) and BM (H) in GPR35^{+/-} and GPR35^{-/-} at steady state. n=4. Data are pooled from 2 independent experiments. (I-K) Quantification of neutrophil (I) and eosinophil (J, K) recruitment index in the lung and spleen of CD45.2 GPR35^{-/-} / CD45.1 GPR35^{+/+} (I) or CD45.2 GPR35^{+/-} / CD45.1 GPR35^{+/+} (J, K) mixed BM chimeras, 12 hrs (I), 4 days (J) or 11 days (K) after intranasal infection. Data are pooled from 2 independent experiments. The chimerism was calculated as the CD45.2⁺ / CD45.1⁺ ratio within blood B220⁺ cells. n=5 (I), n=3-5 (J, K). Data are representative (J) or pooled (I, H) from 2 independent experiments. (L) Flow cytometry histograms showing levels of GPR35 in SiglecF⁺ CD64⁻ CD11b⁺ eosinophils in BM from GPR35^{+/+} (black line) and GPR35^{-/-} (gray line) mice, 11 days after intranasal infection. Data are representative of 2 independent experiments. (M) Transwell migration assay to CXCL12 (100ng/ml) or CCL11 (1μg/ml) of GPR35^{+/+} and GPR35^{-/-} eosinophils isolated from *C. neoformans* infected lung, 11 days after intranasal infection. Nil indicates no added chemoattractant. n=5-8. Data are pooled from 3 independent experiments. (N) Transwell migration assay to 5-HIAA (nM) of control and PTX-treated GPR35^{+/+} eosinophils isolated from *C. neoformans* infected lung 11 days after infection. n=2-3. Nil indicates no added chemoattractant. Data are pooled from 2 independent experiments. * p<0.05; ** p<0.005; *** p<0.0005. Data are presented as mean ± SEM.

Figure S2

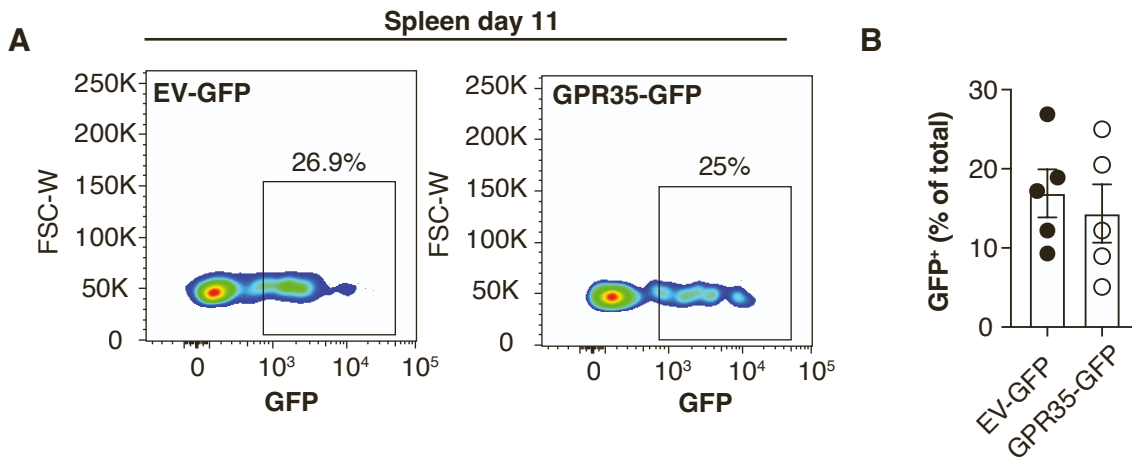
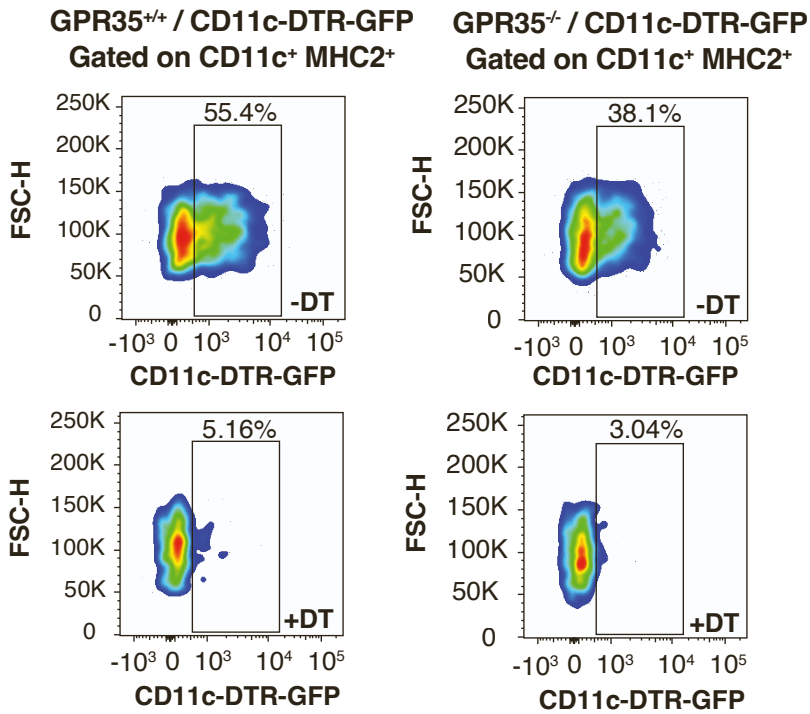


Figure S2, Related to Figure 3. Reconstitution efficiency by retrovirally transduced cells. (A) Flow cytometry plots showing GFP+ percentages out of total splenic cells in *C. neoformans* infected EV-GFP (left) or GPR35-GFP (right) overexpressing BM chimeras, 11 days after intranasal infection. (B) Quantification of splenic GFP+ percentages shown in A. n=5. Data are pooled from 2 independent experiments. Data are presented as mean \pm SEM.

Figure S3

A



B

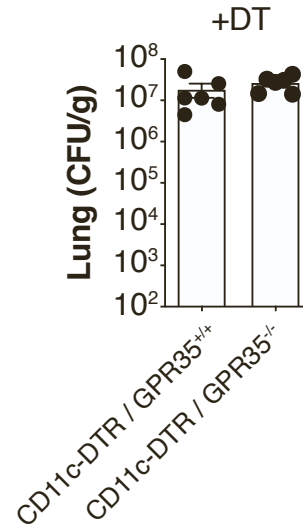


Figure S3, Related to Figure 4. Lack of GPR35-expressing CD11c+ cells does not impact on Cryptococcal burden. (A) Flow cytometry plots showing CD11c-DTR-GFP+ percentages (out of CD11c+ MHCII+ cells) in the lungs of *C. neoformans* infected GPR35^{+/+} / CD11c-DTR-GFP (left) or GPR35^{-/-} / CD11c-DTR-GFP (right) mixed BM chimeras that were either not treated (top) or treated with diphtheria toxin (DT), 11 days after intranasal infection. (B) Quantification of CD11c-DTR-GFP+ percentages shown in A. n=6. Data are pooled from 2 independent experiments. Data are presented as mean \pm SEM.

A

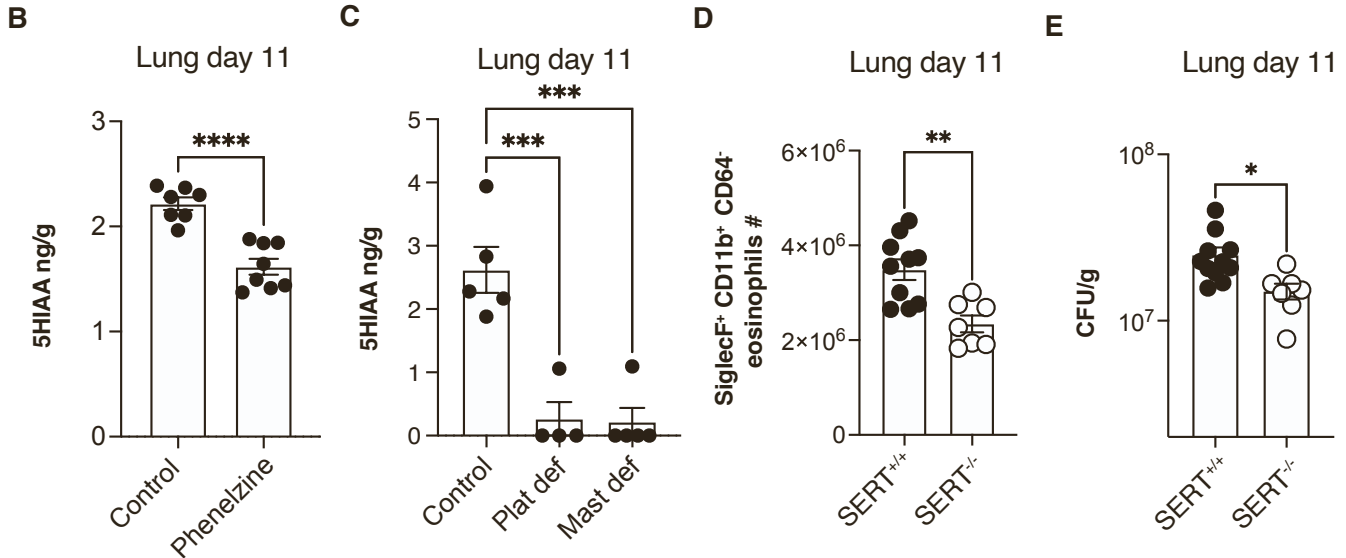
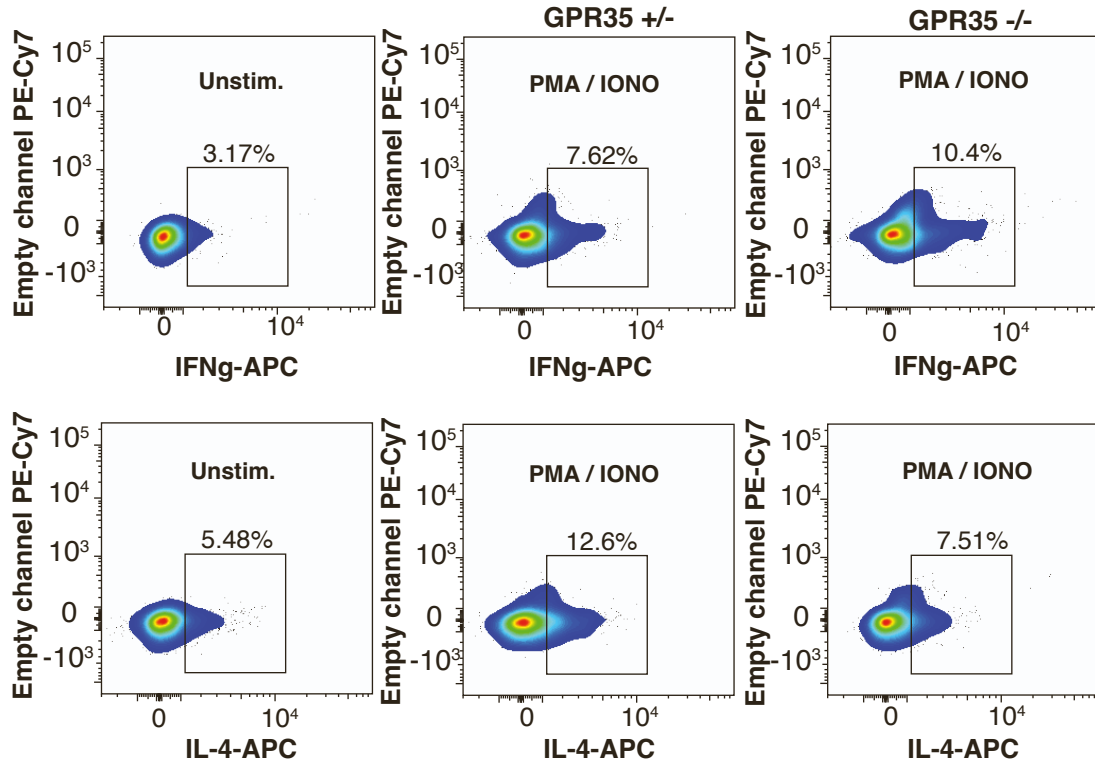
Gated on CD4⁺ CD62L⁻ TCRb⁺ CD4⁺

Figure S4. Related to Figure 4. **Flow cytometric analysis of IFN γ and IL-4 in restimulated T cells from infected lungs (A)** Flow cytometry plots showing controls and ex vivo stimulated (PMA/Iono and Golgi Plug), 3.5hrs stimulation) IFN γ ⁺ (top) and IL-4⁺ (bottom) percentages out of CD4⁺ CD62L⁻ TCRb⁺ CD4⁺ cells in C. neoformans infected lungs of GPR35^{+/+} and GPR35^{-/-} full chimeras, 11 days after intranasal infection. Data are representative of 2 independent experiments. **(B, C)** Quantification by ELISA of 5-HIAA concentrations in the lung of C. neoformans infected mice treated with phenelzine **(B)**, and in the lung of infected platelet (cmlp^{-/-}) or mast cell (Kit^{W/v}) deficient mice **(C)**, 11 days after intranasal infection. n=7-8 (B), n=4-5 (C). Control samples in **(C)** are the same data plotted in **Fig 5A** (Crypto d11 group) and were obtained in parallel with samples from platelet and mast cell deficient mice. **(D, E)** Quantification of SiglecF⁺ CD11b⁺ CD64⁻ eosinophil absolute numbers **(D)** and Cryptococcus CFUs **(E)** in the lung of SERT^{+/+} and SERT^{-/-} mice, 11 days after intranasal infection. n=7-10. Data are pooled from 2 independent experiments. Data are presented as mean \pm SEM.